

UC Irvine

UC Irvine Electronic Theses and Dissertations

Title

Control of Macrophage Function by the Microenvironment

Permalink

<https://escholarship.org/uc/item/3m1953fm>

Author

Smith, Timothy D.

Publication Date

2017

Copyright Information

This work is made available under the terms of a Creative Commons Attribution-ShareAlike License, available at <https://creativecommons.org/licenses/by-sa/4.0/>

Peer reviewed|Thesis/dissertation

UNIVERSITY OF CALIFORNIA,
IRVINE

Control of Macrophage Function by the Microenvironment

DISSERTATION

submitted in partial satisfaction of the requirements
for the degree of

DOCTOR OF PHILOSOPHY

in Biomedical Engineering

by

Timothy Douglas Smith

Dissertation Committee:
Assistant Professor Wendy F. Liu, Chair
Associate Professor Elliot Botvinick
Assistant Professor Michelle Digman

2017

Chapter 2 © 2016 Timothy D. Smith, Margaret J. Tse, Elizabeth L. Read, Wendy F. Liu

All other materials © 2017 Timothy D. Smith

DEDICATION

THOMASINA

God's truth, Septimus, if there is an equation for a curve like a bell,
there must be an equation for one like a bluebell, and if a bluebell,
why not a rose? Do we believe nature is written in numbers?

SEPTIMUS

We do.

—Tom Stoppard, *Arcadia*

TABLE OF CONTENTS

	Page
DEDICATION	ii
TABLE OF CONTENTS	iii
LIST OF FIGURES	iv
LIST OF TABLES	vi
ACKNOWLEDGMENTS	vii
CURRICULUM VITAE	viii
ABSTRACT OF THE DISSERTATION	ix
1. Introduction	1
1.1. Macrophage activation	2
1.2. Macrophage phenotype in wound healing	3
1.3. Tumor-associated macrophages	5
1.4. Macrophage phenotype in the foreign body response	6
1.5. This work	6
2. Regulation of macrophage polarization and plasticity by complex activation signals	7
2.1. Results	10
2.2. Discussion	20
2.3. Methods	25
3. Effects of extracellular matrix identity, ligand density, and activation on macrophage motility	28
3.1. Results	30
3.2. Discussion	39
3.3. Methods	43
4. Conclusions and future directions	45
References	50
Appendix A. Supplement to Chapter 2	61
Appendix B. Supplement to Chapter 3	75

LIST OF FIGURES

Figure 1.1. Ontogeny of macrophages.	1
Figure 1.2. Progression of macrophage phenotype in wound healing.	4
Figure 2.1. Co-stimulation with LPS+IFN- γ and IL-4+IL-13 leads to expression of both CD86 and CD206.	11
Figure 2.2. Co-stimulated macrophages exhibit decreased CD86 expression and increased CD206 expression over time.	13
Figure 2.3. Mathematical modeling of macrophage regulatory logic.	14
Figure 2.4. Multiparametric characterization of macrophage phenotype.	16
Figure 2.5. Macrophage polarization state influences their plastic response to opposing activation signals.	18
Figure 3.1. Motility of unstimulated macrophages on fibronectin.	30
Figure 3.2. Motility of unstimulated macrophages on fibrinogen.	31
Figure 3.3. Combined effects of activation and fibronectin ligand density on macrophage migration.	32
Figure 3.4. Combined effects of activation and fibrinogen ligand density on macrophage migration.	33
Figure 3.5. Integrin expression changes 24 h after macrophage activation.	34
Figure 3.6. Effects of cilengitide on macrophage migration.	35
Figure 3.7. Effects of antibody blockade on macrophage migration.	37
Figure 3.8. Effect of siRNA-mediated integrin knockdown on macrophage motility and shape.	38
Supplementary Figure A1. Expression of phenotypic markers CD86 and CD206 in response to LPS+IFN- γ and IL-4+IL-13 stimuli is dose-dependent.	63
Supplementary Figure A2. Cytokines present in culture media of macrophages exposed to LPS+IFN- γ \pm IL-4+IL-13 for the indicated time in hours, assessed by multiplex ELISA.	64
Supplementary Figure A3. Pulse-chase experiment.	65
Supplementary Figure A4. Simulated timecourse experiment from each model shown in Figure 2.3.	66
Supplementary Figure A5. qRT-PCR timecourse data for Arg1 expression, relative to the IL-4+IL-13-only condition at 24 hours.	67
Supplementary Figure B1. Fibronectin adsorption curve.	75
Supplementary Figure B2. Representative flow cytometry plots of BMDM integrin expression as a function of macrophage polarization.	75

Supplementary Figure B3. Integrin expression changes 24 h after macrophage polarization on different ECMs.

76

LIST OF TABLES

Table 3.1. Mouse BMDM ECM integrins.	29
Supplementary Table A1. qPCR primers	71
Supplementary Table A2. Description of model parameters	72
Supplementary Table A3. Model parameter values	73

ACKNOWLEDGMENTS

This work would not have been possible without the insight, determination, and patience of my advisor, Dr. Wendy Liu.

Throughout, I depended on the friendship and camaraderie of my colleagues in the Liu lab and the Cardiovascular Center, the hosts and guests of 67204, the cyclists of the Taco Tuesday Social Ride, the *not-biology* family, and yet others who defy categorization. Together, we explored the deserts, beaches, bike trails, and mountaintops of California, the \$3 specials at the University Club, and the mysteries, revelations, frustrations, and joys of research. I couldn't have asked for better companions.

I am grateful to Drs. Chris Morse, Joanne Pratt, and Alisha Sarang-Sieminski for introducing me to the beauty of the molecular and cellular worlds, and for their devoted mentorship. It is a testament to his generous nature that Dr. John D. Roberts remained patient and interested while guiding me through my first summer research project.

Thank you, Liang, for everything.

Thank you, Mom, Dad, and Kaitlin, for your love and support, even when I forgot to call.

Esther Chen graciously contributed Figure 1.2. The modeling work described in Chapter 2 was performed by Margaret Tse and Dr. Elizabeth Read. Xiuhui Gao helped collect the cell migration tracks described in Chapter 3. Dr. Vijaykumar Meli provided siRNA-transformed macrophages. Linda McCarthy contributed essential cell culture assistance, moral support, and dogs to pet.

Chapter 2 is reproduced with permission from the Royal Society of Chemistry. Financial support was provided by NSF Graduate Research Fellowship Program grant DGE-1321846 (thanks, Obama!), NIH grant DP2-DE023319 to Wendy Liu, the Center for Complex Biological Systems, and University of California, Irvine.

CURRICULUM VITAE

Timothy Douglas Smith

- 2010 BS in Engineering, Franklin W. Olin College of Engineering
- 2010-11 Boreal Genomics, Vancouver, BC
- 2016 MS in Biomedical Engineering, University of California, Irvine
- 2017 PhD in Biomedical Engineering, University of California, Irvine

FIELD OF STUDY

Macrophage response to biomaterials

PUBLICATIONS

ORCID 0000-0002-5750-0706

Smith TD, Gerken JB, Jog PV, Roberts JD. Conformational equilibria of ethanolamine and its hydrochloride in solution. *Organic Letters*. 2007; 9 (22): 4555-7. doi:10.1021/ol7020077

García AA, Smith TD, Datta R, Luu T, Gratton E, Potma E, Liu WF. Label-free identification of macrophage phenotype by fluorescence lifetime imaging microscopy. *J Biomedical Optics*. 2016; 21(4):46005.

McWhorter FY, Smith TD, Liu WF. A microwell system for detection of secreted products by single adherent cells. *Integrative Biology*. 2016; 8(7):751. doi:10.1039/c6ib00053c.

Smith TD, Tse MJ, Read EL, Liu WF. Regulation of macrophage polarization and plasticity by complex activation signals. *Integrative Biology*. 2016; 8(9):946. doi:10.1039/c6ib00105j.

Hsieh J, Smith TD, Meli VS, Tran TH, Botvinick EL, Liu WF. Differential regulation of macrophage inflammatory activation by fibrin and fibrinogen. *Acta Biomaterialia*. 2016; 47:14. doi:10.1016/j.actbio.2016.09.024.

Smith TD, Nagalla RR, Liu WF. Macrophages in wound healing and regenerative medicine. *Advanced Drug Delivery Reviews*. 2017. In process.

ABSTRACT OF THE DISSERTATION

Control of Macrophage Function by the Microenvironment

By

Timothy Douglas Smith

Doctor of Philosophy in Biomedical Engineering

University of California, Irvine, 2017

Assistant Professor Wendy F. Liu, Chair

Macrophages are versatile cells of the immune system that play an important role in both advancing and resolving inflammation through both signaling and phagocytosis. To perform their diverse functional roles, these cells respond dynamically to cues in their microenvironment. Although macrophage activation has been described as a binary and exclusive polarization to an inflammatory M₁ function or a wound-healing M₂ function, macrophages expressing markers associated with both M₁ and M₂ activity are observed *in vivo*. Using flow cytometry, the macrophage population's response to combined M₁ and M₂ activation signals, presented either simultaneously or sequentially, was assessed. Macrophages exposed to a combination of LPS, IFN- γ , IL-4, and IL-13 acquired a mixed activation state, with individual cells expressing both M₁ marker CD86 and M₂ marker CD206 instead of polarizing to discrete phenotypes. These results corroborate a multidimensional model of macrophage activation and demonstrate that phenotypic markers evolve with time and with exposure to complex signals. Further, the migration of macrophages along extracellular matrix materials characteristic of the wound

environment was explored. Migration speed is sensitive to the composition and concentration of the matrix along which macrophages migrate. Activation with cocktails of LPS and IFN- γ slowed macrophage migration, while treatment with IL-4 and IL-13 directed cells along linear tracks. The effect of macrophage activation on extracellular matrix (ECM) concentration-dependent macrophage migration was characterized and the effect of interrupting integrin-mediated cell-matrix interactions was assessed. Together, the studies help to elucidate the roles of the cytokine and ECM environment in macrophage polarization, plasticity, and migration.

1. Introduction

Macrophages are immune cells with many functions. Macrophages are effector cells, taking up pathogens and debris by phagocytosis and destroying them with enzymes and peroxides; victorious macrophages will present the digested remains of the foreign material to cells of the adaptive immune system to stimulate antibody production. Macrophages also help to coordinate the immune onslaught by acting as signaling transducers and amplifiers, secreting inflammatory or immunomodulatory cytokines into their environment. This signaling role makes macrophages essential for both the advancement and the constructive resolution of inflammation.

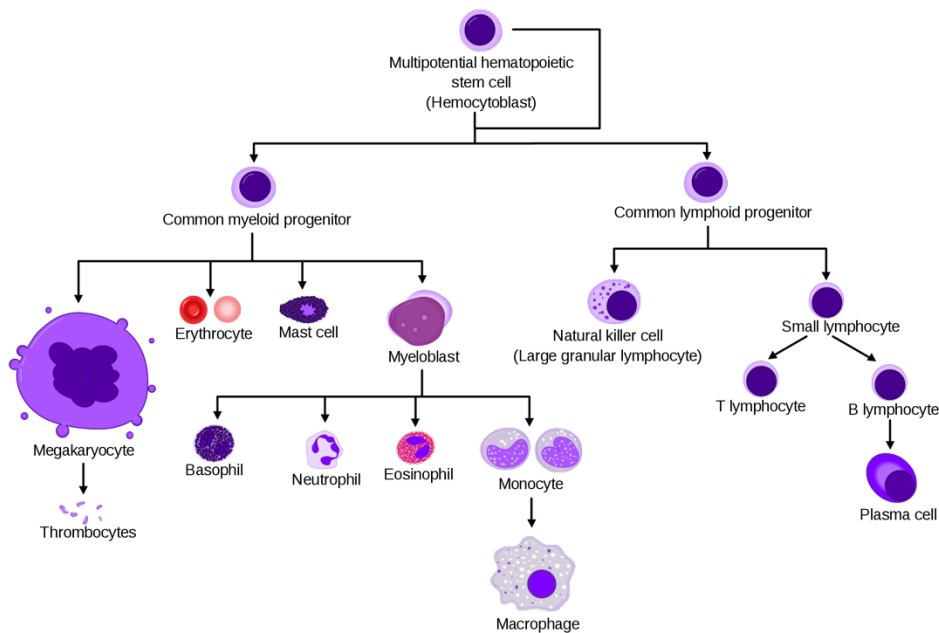


Figure 1.1. Ontogeny of macrophages.
Macrophages arising from blood cells are derived from monocytes. (1)

Most macrophages in inflammatory contexts are derived from circulating monocytes (Figure 1.1). Monocytes mature in bone marrow before entering circulation, where they compose 2-10% of white blood cells (2). Monocytes patrol the circulation for signs of inflammation and respond by extravasation and migration towards the inflammatory signals; as they leave the circulation, monocytes mature irreversibly into macrophages or dendritic cells. Other populations of macrophages, known as tissue macrophages, are permanently resident in tissue and derived from the embryonic yolk sac (3,4). At equilibrium, most macrophages in a tissue are these self-replenishing tissue macrophages, rather than monocyte-derived macrophages (MDMs). The tissue-resident sentinels are quickly outnumbered by recruited MDMs in the presence of danger signals.

1.1. Macrophage activation

Macrophages exhibit stereotyped responses to certain signals in their environment through a process known as activation. Classical, or M₁, activation is induced by recognition of pathogen-associated molecular patterns or the cytokine interferon- γ (5,6). M₁ activation causes macrophages to begin secreting inflammatory cytokines, including TNF- α , and induces profound physiological shifts. Production of free radicals by upregulation of Nos2 is accompanied by a shift in mitochondrial respiration from oxidative phosphorylation to glycolysis (7). M₁-activated mouse MDM also have a distinct flat, round morphology *in vitro* (8). M₁ activation is essential for a robust immune response to pathogens (5).

The discovery of factors that induced a different set of molecules and behaviors in macrophages while appearing to oppose classical activation led to the concept of

alternative, or M₂, activation. The M₁-M₂ nomenclature arose because classical activation is closely associated with interferon- γ , which is secreted by Th₁ cells, and alternative activation was first observed in response to IL-4, which is secreted by Th₂ cells. M₂ macrophages are noted for their constructive participation in matrix organization and tissue repair (6). IL-4-exposed macrophages may be recognized by their increased expression of mannose receptor CD206. In mice, IL-4 treatment drives expression of arginase I, and also leads to an elongated shape *in vitro* (6,8). Other forms of alternative activation have been recognized, leading to a proliferation of “M” notations: M_{2a}, M_{2b}, M_{2c}, Mox, and others (9,10). Indeed, recent work in human MDM identified several macrophage gene modules that can be persistently activated in response to different ligands (11).

Inevitably, the M₁ macrophages produced with IFN- γ and M₂ macrophages produced with IL-4 and IL-13 *in vitro* represent caricatures of the traits of macrophages that exist in complex and dynamic milieus of the body. The M₁/M₂ nomenclature is nonetheless useful in describing macrophages during wound healing and regeneration, because observable changes in M₁ and M₂ markers do correlate with progress towards healing. The M₁/M₂ paradigm also captures the principle that the presence of macrophages may not imply unrestrained inflammation.

1.2. Macrophage phenotype in wound healing

Indeed, normal wound healing is marked by a progression from M₁-like to M₂-like macrophage phenotypes in the wound environment. MDMs play important roles in the wound healing process; animals depleted of monocytes or macrophages exhibit reduced

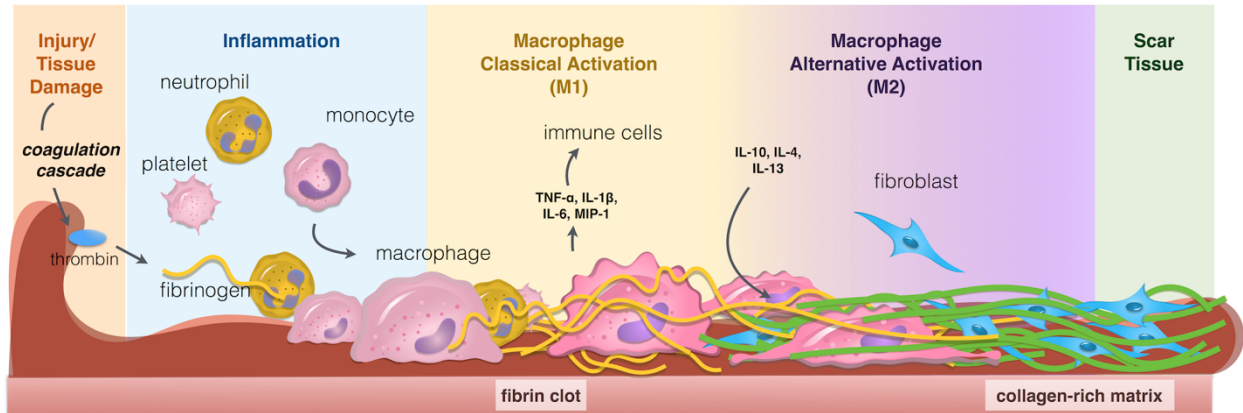


Figure 1.2. Progression of macrophage phenotype in wound healing.

Macrophages arrive in a wound in the first few hours after injury and become activated. Over time, as wounds resolve, macrophages shift from a M1-like phenotype towards a M2-like phenotype. Figure courtesy of Esther Chen.

repair (12,13). M1 macrophages arrive at wounds early and help recruit an effective defense to pathogens (14). Despite their critical early role, chronic M1 activation delays wound healing (15,16). Over time, the emergence of a M2-like macrophage phenotype helps blunt inflammatory activation and organize matrix repair. An example of the necessity of M2 macrophages in healing was shown in *Trib^{-/-}* mice, which have impaired M2 activation of tissue-resident macrophages (17). After an experimental myocardial infarction, *Trib^{-/-}* mice exhibit a deficiency of M2-like CD206⁺ macrophages in the left ventricle and experience delayed cardiac healing—even leading to cardiac rupture—compared to wild type mice (18). Yet, more is not better: unrestrained M2 activity can lead to fibrosis. The M2 role in fibrosis was seen in a study which depleted macrophages systemically in mice during the subacute healing phase after a skin graft. Macrophage depletion at a time when M2-like macrophages were otherwise observed to be present at the graft site reduced scar formation (19).

1.3. *Tumor-associated macrophages*

A particularly egregious dysregulation of the anti-inflammatory macrophage phenotype is observed in tumor-associated macrophages (20). Macrophages form a significant cellular component of many solid tumors (21); tumor macrophage populations are thought to be derived predominantly from circulating monocytes (4). Successful tumors secrete factors including CCL2 that recruit monocytes from blood alongside molecules including CSF₁ and IL-4 that push macrophages away from a tumor-killing phenotype and towards stereotypical M₂ activity. These tumor associated macrophages (TAMs) help to shield and develop the tumor. In even the earliest stages of metastasis, single tumor cells recruit and educate macrophages to protect the nascent metastasis from other components of the immune system (22). In many types of cancer, TAM burden is linked to poor prognosis, and tumorigenesis is limited when macrophages are depleted from animal models (23). The ways TAMs assist their patrons include secreting TGF β , which promotes tumor growth, and IL-10, which is immunosuppressive. TAMs also migrate into hypoxic regions of the tumor and secrete VEGF, which promotes angiogenesis and in turn encourages greater tumor growth (23). Moreover, macrophages are direct enablers of metastasis. Macrophages along the tumor periphery direct metastasis by blazing a trail for tumor cells to follow (24,25). Macrophages have extensive matrix remodeling capabilities and tumor cells are observed to form migrating streams with macrophages to find a path through stromal tissue and into vessels. Tumor cells and macrophages are capable of entering a paracrine signal loop whereby macrophages secrete EGF, which encourages tumor cells to draw near and secrete CSF₁, which

reinforces the macrophage behaviors. Through this process, tumor cells follow macrophages through matrix. Streaming migration behavior has been demonstrated in tumor models *in vivo* with intravital confocal microscopy (26,27) and reconstituted *in vitro* (28).

1.4. Macrophage phenotype in the foreign body response

To biomedical engineers, macrophage phenotype is also important in the context of the macrophage-driven foreign body response to implanted materials (29,30). A chronic M₁-type response can lead to implant failure from chemical attack and poor repair of surrounding matrix and tissue. A chronic M₂-type response is associated with fibrotic encapsulation, which can constrain mechanical devices and disable sensors. Macrophages expressing M₁- and M₂-associated markers are often observed in the vicinity of devices retrieved for histological examination.

1.5. This work

This work extends the body of knowledge about macrophages in two ways. In Chapter 2, I examine the phenomenon of macrophages which express markers of *both* M₁ and M₂ activation. Creating an *in vitro* model for these macrophages, which are often seen in implant studies and in tumor stroma, and exploring how they may arise will improve our ability to assess how implanted materials or TAM-targeted therapies influence macrophage phenotype. In Chapter 3, I undertake a study of the quantitative migration of polarized macrophages on matrices characteristic of the wound environment.

2. Regulation of macrophage polarization and plasticity by complex activation signals

Macrophages are functionally complex cells of the innate and acquired immune system. In addition to their roles as professional phagocytes and antigen-presenting cells, macrophages are sensitive integrators and transducers of biochemical signals with a wide repertoire of responses. A recent study of the macrophage transcriptomic response to a range of stimulatory molecules identified dozens of distinct mRNA coexpression modules (11). Two particular macrophage response patterns which have been widely recognized are the M₁ and M₂ programs, named because they are respectively elicited by products of Th₁ and Th₂ cells (31,32). The M₁ response, also described as classical activation, is typically evoked *in vitro* by treating cells with interferon- γ (IFN- γ) and lipopolysaccharide (LPS), a bacterial cell wall component and TLR₄ agonist. The M₁ phenotype includes production of inflammatory cytokines including TNF- α and IL- 1β (33). M₁ macrophages also undergo a metabolic transition towards glycolysis and secrete free radicals. The M₂ response, also known as alternative activation, is evoked by IL-4 and IL-13 treatment and is characterized by increased expression of CD206, scavenger receptors, and—in mice—arginase 1. The M₂ response has been further classified as the M_{2a} response after other forms of alternative activation were identified. These stereotyped responses are likely only fully recognized *in vitro*, but M₁-like and M₂-like phenotypes are readily identified in physiological contexts.

M₁- and M₂-activated macrophages exhibit characteristic transcriptional and secretory profiles. M₁ activation is associated with STAT₁ and IRF activation, and M₂ activation is associated with STAT6 activity (34). These pathways suppress each other; IL-4-induced STAT6 activation suppresses STAT₁-dependent transcription in mouse macrophages (35), and STAT₁ activation suppresses STAT6-dependent transcription (36). Further, costimulation with IL-4 reduces the IFN- γ -dependent surface expression of Fc γ R on human monocytes (37). Yet, despite the evidence of mutual repression, markers associated with both M₁ and M₂ phenotypes have been observed simultaneously on individual cells *in vivo* (38). This co-expression may reflect simultaneous co-activation of M₁ and M₂ programs. A similar process is observed in T cells, where differentiation of CD4⁺ T cells to IFN- γ -secreting Th₁ cells or IL-4-secreting Th₂ cells in mixed culture conditions yields a tunable continuum of cell fates (39). Modeling revealed that this outcome was consistent with gene regulation governed by a mutual inhibition, self-activation (MISA) network, a common motif thought to govern alternative fate-decisions in many cell types (40), including macrophages (41,42).

M₁ and M₂ marker coexpression may also indicate that cells are shifting from one phenotype to another as the microenvironment changes. Indeed, macrophages have been shown to exhibit phenotypic plasticity *in vitro*. M₁-activated macrophages induced by exposure to bacteria (43) or IFN- γ , alone (44) or in combination with LPS (45), can be re-polarized to express markers associated with an anti-inflammatory phenotype upon subsequent treatment with IL-4, alone or in combination with IL-13. Similarly, macrophages treated with IL-4 will express inflammatory markers upon subsequent

treatment with LPS or IFN- γ (43). The plasticity of these influential cells has made them an attractive target for immunomodulation; scaffolds and materials that achieve controlled delivery of macrophage-activating agents is an active area of research for treatment of diseases involving macrophage dysregulation (reviewed in Ref. (46)). In atherosclerosis, sustained inflammation exacerbates oxidative stress in the plaque (47). Plaque shoulders, which are prone to rupture, are typically dominated by macrophages expressing markers associated with M1 activation (38). Reprogramming macrophages toward a M2 phenotype may prevent plaque rupture and promote plaque resolution by encouraging matrix deposition (48,49). In the case of cancer, tumor-associated macrophages (TAMs) are thought to induce anti-inflammatory signaling that helps protect the tumor from immune assault (23). Recent evidence suggests presenting M1-activating factors to TAMs can help engage the immune system to attack the tumor (50). An improved understanding of how macrophages respond to stimuli that redirect their phenotype should help develop better therapeutic approaches for these important pathologies.

In this study, we investigated how treatment with mixed M1 and M2 stimuli, either simultaneously or sequentially, regulates macrophage phenotype. We were motivated to understand whether a mixed phenotype represents a superposition of the M1 and M2 phenotypes, a transition between states, or, as some findings have suggested (51), a unique mixed program. To consider the expression state of individual cells, we used flow cytometry to assay surface expression of M1 marker CD86 and M2 marker CD206. Mouse bone marrow derived macrophages were stimulated with LPS+IFN- γ and/or IL-4+IL-13 at

various doses over durations of 24-96 hours. Our findings suggest that macrophages adopt a mixed phenotype dependent on the relative strength of stimuli present, and that cells progress towards a M2 phenotype over time. These temporal changes in expression were found to be consistent with a mathematical model comprising a modified MISA network. In addition, reprogramming of macrophages to the opposing phenotype is dependent on the extent of pre-polarization. More specifically, expression of CD206 in response to IL-4+IL-13 is enhanced by pre-polarization towards an M1 phenotype with LPS+IFN- γ . In contrast, expression of CD86 in response to LPS+IFN- γ , particularly at low doses, is inhibited by pre-polarization towards an M2 phenotype with IL-4+IL-13. Together, these data provide evidence of a macrophage phenotypic continuum by analysis of phenotypic markers at the single cell level, and suggest that macrophage reprogramming by combined activation signals is dependent on initial polarization state and dosage of stimulation.

2.1. Results

2.1.1. Co-stimulated macrophages express markers of both M1 and M2 activation

We first sought to establish a dose range that would yield a submaximal response to facilitate detection of enhancement and repression effects. We exposed mouse bone marrow derived macrophages (BMDM) to varying doses of stereotypical M1 (LPS+IFN- γ) or M2 stimuli (IL-4+IL-13). To maximize the sensitivity of our assays, we selected doses from 0 to 0.3 ng/ml for LPS+IFN- γ and 0 to 1 ng/ml for IL-4+IL-13 based on a pilot experiment suggesting that doses in these ranges did not completely saturate expression of CD86 and CD206. Cells were exposed to stimulus for 48 hours and assayed for

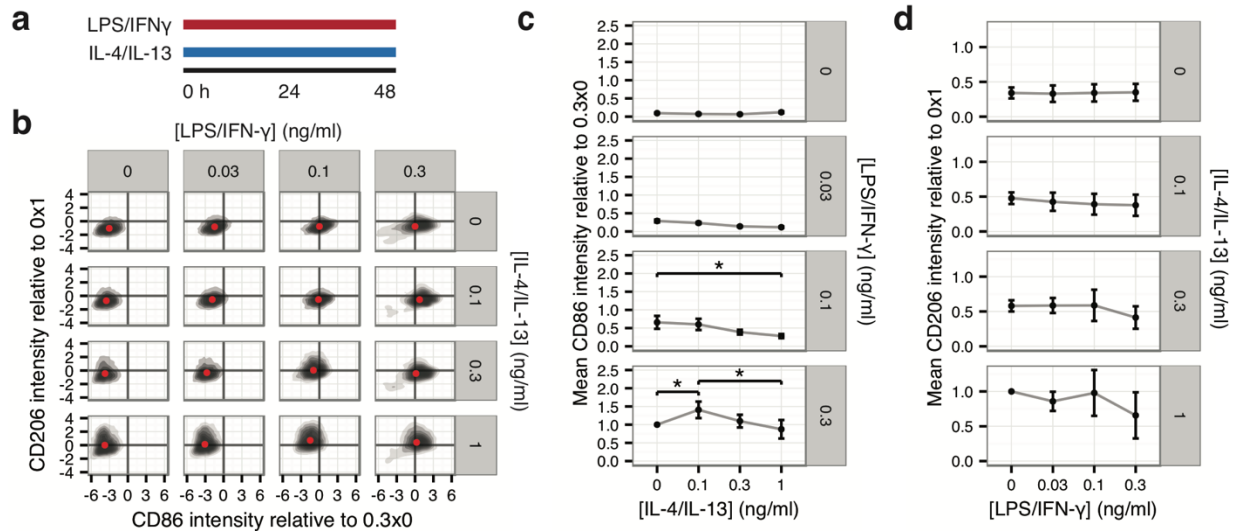


Figure 2.1. Co-stimulation with LPS+IFN- γ and IL-4+IL-13 leads to expression of both CD86 and CD206.

(a) Schematic illustrating experimental conditions. Macrophages were exposed to LPS+IFN- γ and/or IL-4+IL-13 for 48 hours before analysis. (b) Density plots of normalized CD206 versus CD86 staining intensity of macrophages subjected to different concentrations of LPS+IFN- γ and/or IL-4+IL-13 (ng/ml) for 48 hours, assessed by flow cytometry. CD86 is normalized to the LPS+IFN- γ -only condition and CD206 is normalized to the IL-4+IL-13-only condition. Representative plots from a single experiment. Median position is indicated by a red dot. (c) Average median normalized CD86 intensity \pm SEM ($n = 3$) of LPS+IFN- γ treated cells vs. co-added IL-4+IL-13 dose, grouped by LPS+IFN- γ dose, normalized per experiment as in B. (d) Average median CD206 intensity \pm SEM ($n = 3$) of IL-4+IL-13 treated cells vs. co-added LPS+IFN- γ stimulus, grouped by IL-4+IL-13 dose, normalized per experiment as in B. Asterisk indicates significant difference by two-sided t test, $p < 0.05$.

expression of M₁ marker CD86, a T-cell costimulatory molecule, and M₂ marker CD206, a mannose receptor, by flow cytometry. We found that median CD86 labeling intensity increased tenfold as the dose of LPS+IFN- γ was increased from 0 to 0.3 ng/ml (Supplementary Figure A1a and b). Labeling intensity of CD206 increased threefold as IL-4+IL-13 was increased from 0 to 1 ng/ml (Supplementary Figure A1c and d). At these concentration ranges, the expression of phenotypic markers was not saturating, so that the expression of markers generally increased with stimulation dose.

To explore the effect of co-stimulation with M₁ and M₂ activation signals on macrophages, BMDM were exposed simultaneously to combinations of LPS+IFN- γ and

IL-4+IL-13 at doses in the determined range for 48 hours. Expression of CD86 and CD206 was analyzed by flow cytometry (Figure 2.1a and b). Notably, the population remained single-peaked in plots of CD86 expression vs CD206 expression, and did not show separation into distinct subpopulations. Cells generally did not individually commit to exclusive CD86 or CD206 expression. Indeed, CD86 and CD206 expression were only partially inhibited by exposure to their opposing polarization signal. Analysis of CD86 expression in LPS+IFN- γ -stimulated cells (0.3 ng/ml) showed that moderate amounts of co-added IL-4+IL-13 (0.1 ng/ml) in fact increased the median expression of CD86 40% (\pm 22% SEM, n=3). Further increasing the IL-4+IL-13 dose to 1 ng/ml abrogated this enhancement. Meanwhile, the expression of CD206 in IL-4+IL-13 stimulated cells was not affected by the co-addition of LPS+IFN- γ stimuli at any dose (Figure 2.1d). In sum, these data demonstrate that macrophages exposed to combinations of the activation signals LPS+IFN- γ and IL-4+IL-13 express both CD86 and CD206 at 48 h of stimulation, and repression of the contrasting pathway was only partially observed with these phenotypic markers.

2.1.2. Co-stimulated macrophages progress towards a M2-like phenotype

To examine how macrophage phenotype evolves over time after exposure to stimulus, we exposed BMDM to stereotypical M₁, M₂, or mixed stimuli, and examined CD206 and CD86 expression at 24 hour intervals for 96 hours (Figure 2.2a). In conditions containing LPS+IFN- γ , including the mixed condition, cells began to express more CD206 and less CD86 over time. The IL-4+IL-13-only and no-treatment conditions exhibited a transient increase in CD206 that peaked at 48 hours, and relatively low and stable CD86 expression

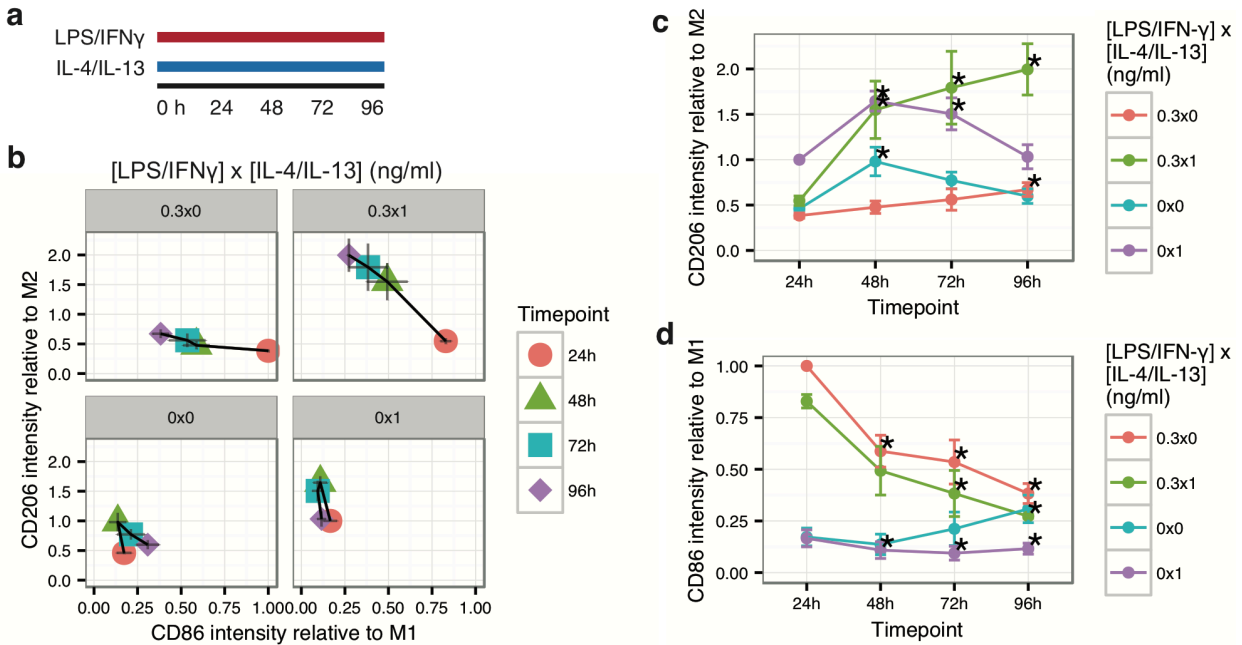


Figure 2.2. Co-stimulated macrophages exhibit decreased CD86 expression and increased CD206 expression over time.

(a) Schematic illustrating experimental conditions. Macrophages were exposed simultaneously to LPS+IFN- γ and/or IL-4+IL-13 for 24, 48, 72, or 96 hours. Each experiment used BMDM isolated from a single mouse. (b) Expression of CD206 versus CD86 of different stimulation conditions over time. Average of median population location \pm SEM ($n=5$) is shown. (c) Expression of CD86 staining intensity over time for different stimulation conditions, normalized to the intensity of LPS+IFN- γ condition at 24 hours. Average of median population location \pm SEM ($n=5$) is shown. Asterisk indicates difference vs 24 hours by two-sided t test, $p < 0.05$. (d) Expression of CD206 staining intensity over time for different stimulation conditions, normalized to the intensity of IL-4+IL-13 condition at 24 hours. Average of median population location \pm SEM ($n=5$) is shown. Asterisk indicates difference vs 24 hours by two-sided t test, $p < 0.05$.

(Figure 2.2b). In cells treated only with LPS+IFN- γ , the expression of CD86 decreased over the course of the 96 hour time period with the greatest decrease occurring between 24 and 48 hours (Figure 2.2c). Macrophages exposed to mixed LPS+IFN- γ and IL-4+IL-13 stimulation also displayed a decrease in CD86 expression, which was similar in profile to that of cells stimulated with only LPS+IFN- γ . In contrast, CD206 expression in response to IL-4+IL-13 increased up to 48 hours after stimulation, and then subsequently decreased after 72 hours, but the levels remain elevated when compared to expression in unstimulated macrophages even at 96 hours (Figure 2.2d). The extent of decrease was similar, but occurred at earlier time points, when the stimulus was washed out after 24

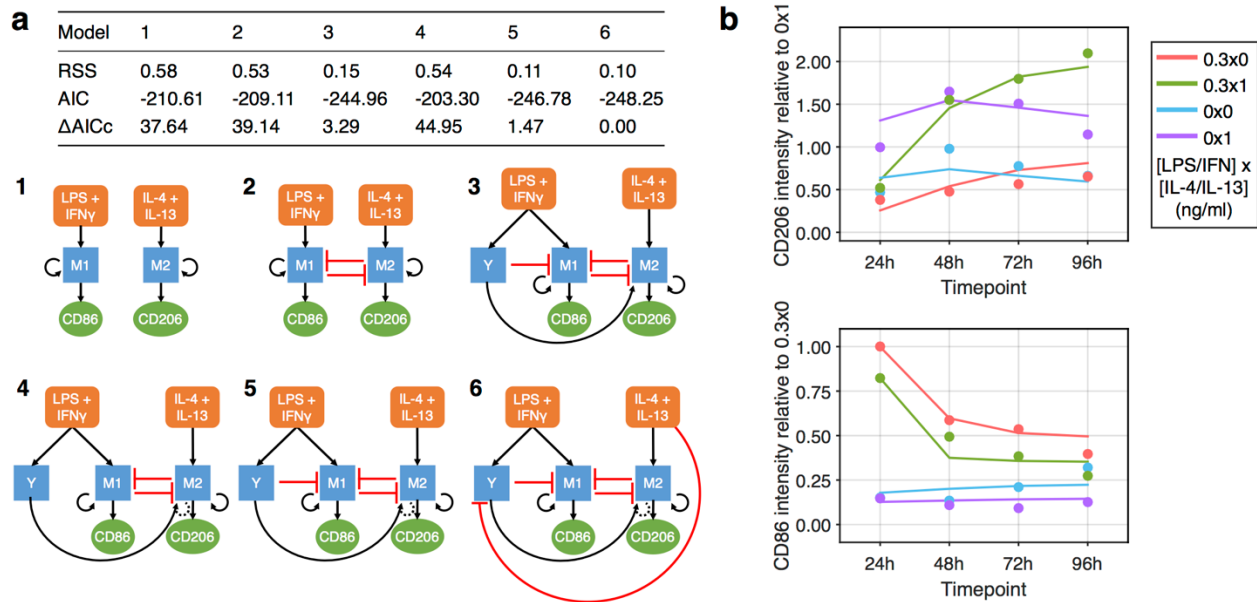


Figure 2.3. Mathematical modeling of macrophage regulatory logic.

(a) A representative set of minimal models for activation of M₁ and M₂ pathways under costimulation, comprised of a modified MISA (Mutual Inhibition/Self-Activation) network. Y: an unspecified regulator. Dashed line indicates that positive regulation of M₂ by Y occurs cooperatively with M₂. Models are shown in order of increasing number of parameters. RSS score indicates goodness of fit, and AIC score measures model quality, while penalizing presence of additional parameters. Δ AICc is reported relative to best (lowest) value, corresponding to Model 6. In general, successful models (3,5, and 6) incorporated both an incoherent feed-forward loop on M₁ and positive regulation of M₂, mediated by Y. (b) Simulated expression of CD86 and CD206 stimulated with LPS+IFN- γ and/or IL-4+IL-13 for 24, 48, 72, or 96 hours. Simulated data are from the model with both the best AICc and RSS score, Model 6, fit to the normalized time course data.

hours (Supplementary Figure A₃). Interestingly, mixed stimulation conditions induced a marked increase in CD206 expression, which was significantly enhanced relative to the cells stimulated with only IL-4+IL-13.

2.1.3. Modeling proposes a complex interdependence of M₁- and M₂-associated pathways

In order to gain further insight into the logic of macrophage activation, we performed mathematical modeling of CD86 and CD206 expression in response to the different co-stimulatory conditions. Our modeling strategy was designed to identify the key features of the regulatory logic linking CD86 and CD206 expression (“outputs”) to stimulation by

LPS+IFN- γ and/or IL-4+IL-13 (“inputs”). To this end, we analyzed a suite of candidate models and performed model selection based on fitting to the experimental 96-hour timecourse data (Figure 2.3). Mathematical descriptions of the models are provided as Supplementary Equations in Appendix A; the parameters are described in Supplementary Table A2 and the best-fit values are given in Supplementary Table A3. Rather than treating signaling and gene regulatory networks in detail (as quantitative parameters remain unknown), the network models comprise a small number of interacting nodes representing inputs, outputs, and M₁- and M₂-associated pathways. Models of T cell specialization (39,52,53) and fate-decisions in diverse cell types (40) commonly employ a core Mutual Inhibition, Self-Activation (MISA) network motif. We found that the basic MISA motif was insufficient to reproduce the observed temporal expression patterns, including the decrease of CD86 expression after 24 hours and the sharp increase of CD206 after 24 hours under co-stimulatory conditions.

We explored a number of additional small-network topologies, consistent with current knowledge of macrophage activation pathways. In the MISA paradigm, costimulus results in a mixed response, in which both markers are expressed simultaneously, albeit at a somewhat reduced level as compared to the strongly polarized case. While the temporal expression of CD86 shows this behavior (dampened, but qualitatively similar kinetics, with addition of IL-4+IL-13), the CD206 kinetics suggests a more complex response to costimulation. We found that successful models (as assessed by either the error or the AICc information criterion) required at least two features extending the core MISA: an incoherent feed-forward loop on the M₁ pathway, and a

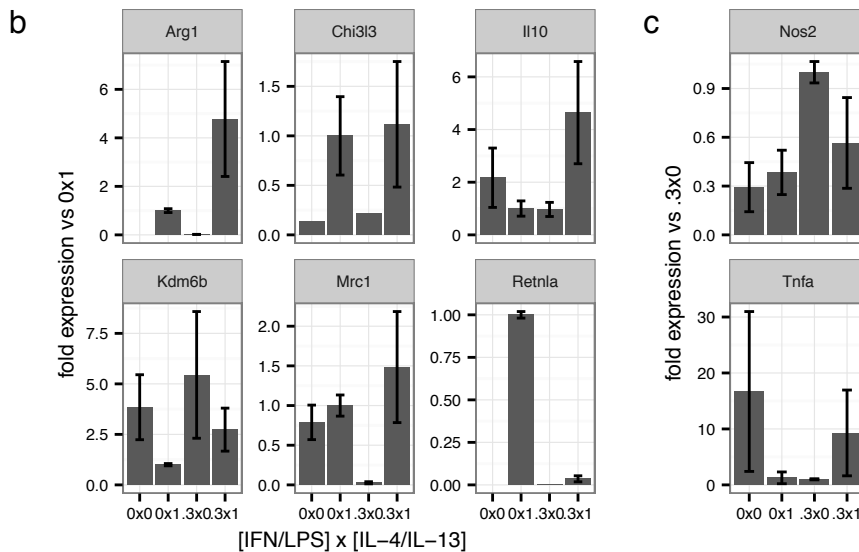
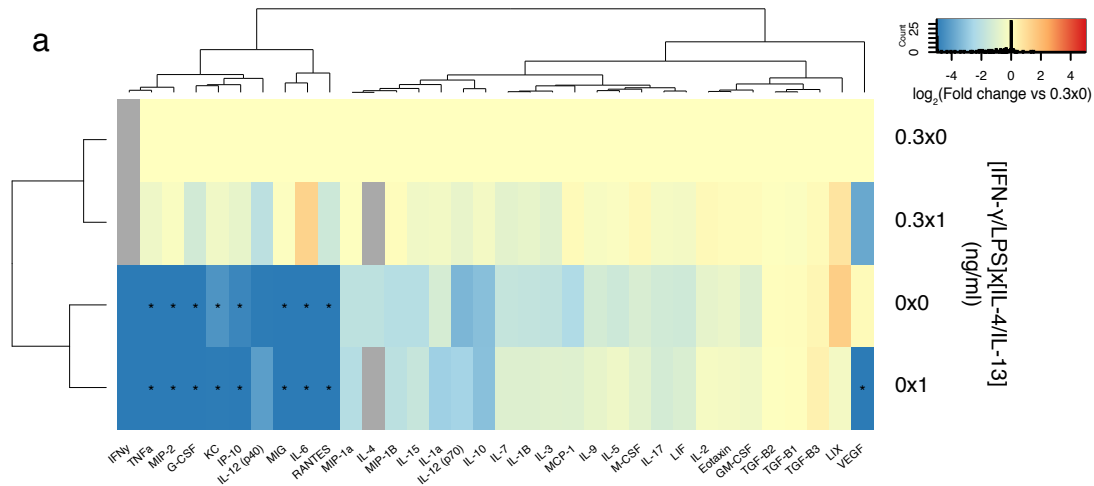


Figure 2.4. Multiparametric characterization of macrophage phenotype.

(a) Dendrogram and heat map of cytokine release from macrophage cultures exposed to LPS+IFN- γ and/or IL-4+IL-13 for 24 hours. All conditions are normalized to inflammatory stimulus. * indicates difference from LPS+IFN- γ -only condition by two-sided t test with Holm correction, $p < 0.05$. Average of 3 experiments. (b) Mean \log_2 transformed fold difference mRNA expression vs. (B) IL-4+IL-13 only or (C) LPS+IFN- γ -only stimulation condition at 24 hours. Missing values indicate amplification below limit of detection. $n = 3$.

mixed (both inhibiting and activating) character of M2 regulation by the M1-axis

(Figure 2.3, Supplementary Figure A3). In the network models, these interactions are mediated by a single additional intracellular regulator (labelled Y). The predictions of the candidate model are presented alongside experimental results in (Figure 2.3b). Details of the mathematical modeling can be found in Appendix A.

2.1.4. Multiparametric characterization of macrophage phenotype

To assess whether the expression of CD86 and CD206 are representative of macrophage function, we performed a multiplexed cytokine assay. We found that macrophages stimulated with LPS+IFN- γ alone for 24 hours exhibited the highest secretion of inflammatory cytokines including IL-6, IP-10, MIG, MIP-1a, MIP-2, MIP-1B, RANTES, and TNF- α , which were found at much lower levels in the supernatants of unstimulated cells or cells exposed only to IL-4+IL-13 (Figure 2.4a). Cells that were stimulated with mixed LPS+IFN- γ and IL-4+IL-13 secreted somewhat lower levels of inflammatory cytokines, with the greatest proportional decrease observed in G-CSF, IL-6, IL-12, IL-15, and TNF- α . Cytokines that were expressed in greater quantity by M₁-stimulated cells compared to naïve cells were also expressed by cells exposed to mixed stimuli. This was consistent with a moderate but significant ($17\% \pm 3.5\%$ SEM, n=6) decrease in CD86 expression in cells treated with mixed cytokines compared to the LPS+IFN- γ only condition at 24 hours (Figure 2.4c). Examining cytokines typically associated with M₂ macrophages, we found that IL-10 was elevated, though not significantly, in the LPS+IFN- γ -only and mixed conditions. TGF- β 1 and 2 expression was similar among all conditions examined. VEGF was strongly suppressed in conditions containing IL-4+IL-13. Indeed, none of the analytes in the ELISA panel were preferentially produced by IL-4+IL-13 treated cells.

We also examined expression of genes associated with M₂ (Figure 2.4b) and M₁ (Figure 2.4c) activation by RT-qPCR at 24 h after stimulation. Transcript expression of *Cd206* as well as *Arg1* showed an increase in expression in mixed cytokine conditions compared to IL-4+IL-13-only conditions (Figure 2.4b).

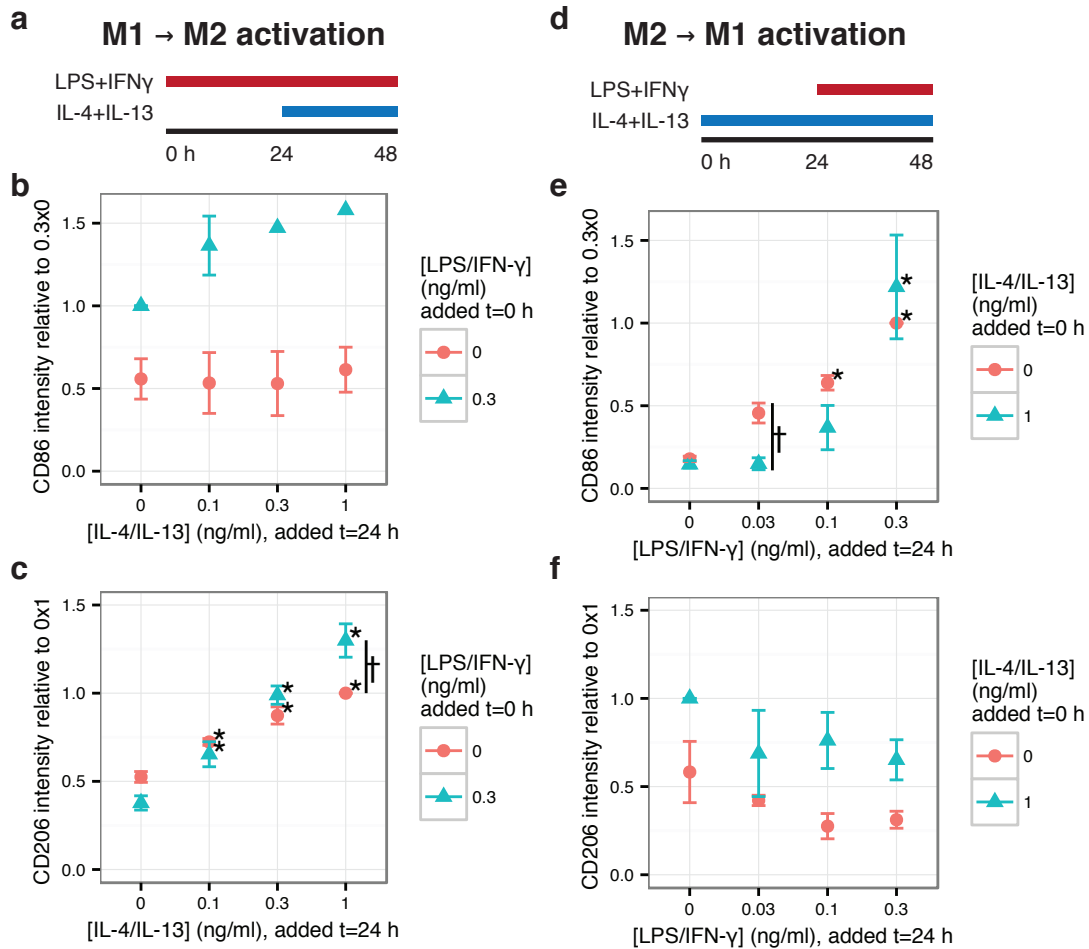


Figure 2.5. Macrophage polarization state influences their plastic response to opposing activation signals.

(a) Schematic illustrating experimental conditions. Macrophages were stimulated for 24 hours with inflammatory stimuli alone before anti-inflammatory stimuli were added for an additional 24 hours, and then assayed.

(b) Expression of CD86 in cells either pre-treated with 1 ng/ml LPS/IFN- γ or untreated for 24 hours and then subsequently treated with IL-4/IL-13 at the indicated dosages. Data are normalized to CD86 expression in 0.3 ng/ml LPS/IFN- γ -only condition, mean \pm SEM ($n=4$).

(c) Expression of CD206 in the same conditions as B. Data are normalized to CD206 expression in 1 ng/ml IL-4/IL-13-only condition, mean \pm SEM ($n=4$).

(d) Schematic illustrating experimental conditions. Macrophages were stimulated for 24 hours with anti-inflammatory stimuli alone before inflammatory stimuli were added for an additional 24 hours, and then assayed.

(e) Expression of CD86 in cells either pre-treated with 1 ng/ml IL-4 and IL-13 or untreated for 24 hours and then subsequently treated with LPS and IFN- γ at the indicated dosages. Data are normalized to CD86 expression in 0.3 ng/ml LPS/IFN- γ -only condition, mean \pm SEM ($n=3$).

(f) Expression of CD206 in the same conditions as E. Data are normalized to CD206 expression in 1 ng/ml IL-4/IL-13-only condition, mean \pm SEM ($n=3$). Asterisks indicate significant differences compared to unstimulated cells by two-sided t test, $p < 0.05$. Dagger indicates differences between groups with and without pre-treatment by two-sided t test, $p < 0.05$.

However, expression of *Retnla* (*Relma*/*Fizz1*) and *Chi3l3* (*Ym1*) was highest in the IL-4+IL-13-only condition, and co-addition of LPS+IFN- γ inhibited expression of these genes, suggesting that M2 markers may be heterogeneously expressed. Expression of *Nos2* was highest in the LPS+IFN- γ only condition. *Tnfa* levels were lower in the LPS+IFN- γ condition compared to the unstimulated and mixed stimulus conditions at the examined timepoint (Fig. 4c), perhaps due to refractory downregulation after stimulation: *Tnfa* is coinduced with genes that degrade *Tnfa* transcripts, leading to a short transcript half-life (54), and activity at the *Tnfa* promoter stops by 18 hours after stimulation with LPS (55).

2.1.5. Macrophage state impacts reprogramming by a second activation signal

It is thought that macrophages in wound environments are plastic and can transition from M1-like to M2-like states as signals in their environment change (13) or are presented by therapeutic materials (46). To investigate this transition *in vitro*, we examined how pre-exposure of macrophages to an inflammatory stimulus influences their response to IL-4 and IL-13. Macrophages were treated with LPS+IFN- γ for 24 hours before IL-4+IL-13 were added for an additional 24 hours. Cells were assayed for CD86 and CD206 expression (Figure 2.5a). We found that expression of CD86 in LPS+IFN- γ pre-treated macrophages showed a modest and non-statistically significant increase in response to subsequent addition of IL-4+IL-13 (Figure 2.5b). In addition, pre-treatment of cells with LPS+IFN- γ did not block expression of CD206 upon IL-4+IL-13 stimulation, and thus cells pre-polarized to a M1 phenotype were still capable of acquiring characteristics of a M2 phenotype (Figure 2.5c). Interestingly, at high doses of subsequent IL-4+IL-13 cytokine

addition, the extent of CD206 expression was 30% (\pm 9% SEM, $n=5$) higher in LPS+IFN- γ pretreated cells when compared to unpretreated cells. These data demonstrate that pre-polarization towards an M₁ phenotype with LPS+IFN- γ does not prevent subsequent M₂ response to IL-4+IL-13, and in fact can enhance the expression of the M₂ marker CD206.

Conversely, perturbing M₂-like macrophages towards a M₁-like phenotype could be therapeutically useful in diseases including cancer, where reprogramming tumor-associated macrophages may help to inhibit tumor growth. To test M₂-to-M₁ plasticity *in vitro*, we pre-treated macrophages with IL-4+IL-13 for 24 hours, added LPS+IFN- γ for a subsequent 24 hours, and assayed cells for CD86 and CD206 expression (Figure 2.5d). We found that at high doses of LPS+IFN- γ , pre-treatment with IL-4+IL-13 did not affect CD86 expression when compared to naïve cells, suggesting that M₂ pre-polarization does not impact reprogramming towards an M₁ phenotype. However, pre-treatment with IL-4+IL-13 inhibited the expression of CD86 upon exposure to low doses of LPS+IFN- γ (Figure 2.5e). CD206 expression was modestly decreased in response to subsequent addition of LPS+IFN- γ in both the IL-4+IL-13 pre-treated and naïve conditions, although these differences were not statistically different (Figure 2.5f). These data suggest that the ability of macrophages to acquire M₁-like behavior after entering a M₂-like state is dependent on the dosage of subsequent M₁ stimulation, and that high doses may be necessary for reprogramming than for initial activation of naïve cells.

2.2. Discussion

We demonstrate that simultaneous exposure of macrophages to mixed cytokines leads to expression of both CD86 and CD206 in individual cells, which are established markers of

M₁ and M₂ activation, respectively (56–59). With 48 hours of stimulation, small quantities of co-added IL-4+IL-13 stimuli enhanced CD86 expression in LPS+IFN- γ -stimulated cells, whereas greater IL-4+IL-13 concentrations inhibited this enhancement. However, high concentrations of stimulus in the mixed condition induced expression of CD86 equivalent to expression in the LPS+IFN- γ -only condition, and expression of CD206 equivalent to expression in the IL-4+IL-13-only condition. Individual cell expressions of CD86 and CD206 expression formed single-peaked, broad distributions, suggesting that individuals do not strongly polarize in mixed cytokine environments. Consistent with this, analysis of the secretome of these populations showed that the presence of IL-4+IL-13 along with LPS+IFN- γ only moderately dampens the level of inflammatory cytokine secretion when compared to LPS+IFN- γ only stimulated cells.

Although both M₁ and M₂ markers are present upon co-stimulation, their evolution over time is different. In cells stimulated in mixed conditions, the M₁ marker CD86 decreases after the first 24 hours and returns almost to basal levels after 96 hours, whereas the M₂ marker CD206 continues to increase peaking at 48-72 hours, and remained sustained relative to unstimulated macrophages even after 96 hours. This difference may be indicative of the natural progression of macrophages from inflammatory to anti-inflammatory phenotype during a host response to a wound or infection with pathogen (13). Unexpectedly, macrophages exposed to mixed conditions had higher levels of CD206 when compared to cells treated with IL-4+IL-13 alone at the longer timepoints, suggesting that presence of an inflammatory stimulus may enhance the long term wound healing response. M₂ marker *Arg1* transcripts measured by

qRT-PCR were also elevated at each time point in the mixed stimulation condition, compared to IL-4+IL-13-only (Supplementary Figure A5).

Our results suggest that macrophage reprogramming to a contrasting phenotype is dependent on initial polarization state and the strength of the second signal. For cells polarized towards an inflammatory phenotype with LPS+IFN- γ , CD206 expression with IL-4+IL-13 was enhanced compared to naïve cells. In contrast, cells polarized to an anti-inflammatory state with IL-4+IL-13 were more resistant to reprogramming with LPS+IFN- γ towards CD86 expression. This effect was observed specifically at the lower LPS+IFN- γ doses; expression of CD86 with high LPS-IFN γ doses was not significantly different between pre-polarized and naïve cells. These data suggest the anti-inflammatory phenotype is enhanced by an initial inflammatory signal, and that macrophage progression from M1-like to M2-like phenotypes is favored.

While exploring signaling network topologies that could model macrophage responses, we discovered that the basic MISA motif was insufficient to account for the complex temporal expression patterns of CD86 and CD206, despite suggestions that elements of mutual inhibition and self activation may play a role in macrophage polarization (41,42). The mathematical models shed light on regulatory interactions which enable macrophages to achieve a spectrum of polarization states, depending quantitatively on microenvironmental cues. The models also suggest a regulatory logic by which individual cells co-stimulated by M1 and M2 signals can achieve transient M1 character followed by progression to a M2 phenotype. Although each node in the small-network models represents the combined action of many species, 'M1' and 'M2' likely reflect (at least in

part) regulation by STAT1 and STAT6, respectively, consistent with their mutual antagonism induced by LPS-IFN γ and IL-4+IL-13 (35–37,60–62). For construction of a parsimonious model in order to avoid overfitting, a single additional node ('Y') was introduced to mediate both the transient nature of CD86 expression, and the mixed inhibiting/activating effect of LPS-IFN γ on CD206. As such, 'Y' likely comprises feedback inhibition mechanisms, including those mediated by SOCS and STAT3 (reviewed in ref. (63)). Furthermore, 'Y' may reflect regulation by NF κ B, which is activated by LPS (64) and inhibited by IL-4 (41). Several studies have suggested a cooperative interaction between NF κ B and STAT6 to promote genes downstream of IL-4 (65–68). Incorporating these interactions into the mathematical model enabled us to construct small networks that captured the temporal response to both mixed and polarizing stimuli. A limitation of this approach is that the model is trained on two markers, which captures only some of the changes associated with macrophage activation. A more comprehensive dataset could lead to a more predictive model at the cost of increasing the complexity of the model.

A discrete "M₃" or "switch" phenotype has been proposed to account for macrophage transitions from M₁-like to M₂-like in the presence of M₁-inducing stimuli, or from M₂-like to M₁-like in the presence of M₂-inducing stimuli (69). The M₃ state is hypothesized to yield an inverted, paradoxical response to stimuli. Stimulating M₃ macrophages with polarizing factors should induce the opposite of the expected phenotype. Although we observe evolution of a M₂-like response characterized by CD206 expression under continued treatment with M₁-inducing factors, our mathematical model suggests that these transitions may be possible in the absence of a distinct switching state.

These findings may have implications for therapeutic strategies involving macrophage reprogramming. For modulating the host response to biomaterial implants, delivery of IL-4 and IL-13 has been shown to increase expression of CD206 in surrounding macrophages (70). Our results suggest that additional delivery of inflammatory cytokines, either concurrently or beforehand, may enhance anti-inflammatory activation and potentially improve the wound healing response. Along these lines, Spiller *et al.* recently demonstrated that delivery of IFN- γ increases angiogenesis in response to a decellularized bone implant (71). For cancer treatment, reprogramming tumor associated macrophages, which are thought to be anti-inflammatory, towards an inflammatory phenotype may require high doses of inflammatory stimuli, since low dosages were not sufficient to induce this transition.

In summary, we find that macrophages exposed to both M₁ and M₂ activation signals express markers of both phenotypes, but the M₁ markers decay over time while the M₂ markers remain elevated. The distribution of markers suggest that macrophages do not exist in discrete polarized states. In addition, acquisition of the M₂ phenotype appears to be enhanced by additional exposure to inflammatory stimulus, suggesting that inflammatory insult potentiates the wound healing response. Together, these results provide a better understanding of macrophage behavior in response to opposing activation signals, which is likely to be involved in the dynamic immune response to pathogens or injury. This improved understanding of macrophage activation will likely help design strategies for treatment of disease in which macrophages are involved.

2.3. Methods

2.3.1. Cell isolation and culture

Primary bone marrow derived macrophages were obtained by harvesting marrow from femurs of 6-12 week old female C57BL/6 mice, lysing red blood cells with ACK buffer, and then culturing cells for seven days on bacteriological polystyrene plates in DMEM supplemented with 10% FBS, 2% penicillin/streptomycin, 2 mM L-glutamine, and 10% conditioned media from CMG 12-14 cells expressing recombinant mouse M-CSF. Macrophages were treated with the indicated doses of LPS (Sigma), IFN- γ , IL-4, or IL-13 (all from Biolegend) for the indicated time.

2.3.2. Flow cytometry

Cells were fixed in 4% formaldehyde and stored at 4 °C until staining with anti-CD86 (clone GL-1, APC conjugate; Tonbo Biosciences) and anti-CD206 (clone Co68C2, Alexa 488 conjugate; Biolegend) antibodies or isotype controls. Cells were analyzed on a BD LSR flow cytometer with post-processing in FlowJo (Tree Star). Cell populations were gated on forward and side scatter to select intact single cells. Events were acquired until 10,000 events were collected in a preliminary analysis gate or the sample was exhausted.

2.3.3. Cytokine analysis

Macrophages were plated at 3e5 cells/ml, allowed to adhere overnight, and treated with indicated doses of IL-4, IL-13, TNF- α , and IFN- γ . Supernatants were collected at 24, 48, 72, and 96 hours after stimulation and analyzed with a Luminex 31-plex mouse cytokine array (Eve Technologies). Hierarchical clustering was performed in R using a complete linkage method and presented with the gplots package (72).

2.3.4. RT-PCR

For gene expression analysis, cells were lifted from culture plates 24 hours after stimulation, pelleted by centrifugation, and frozen at -80°C . Cells were lysed and RNA was extracted with the Qiagen RNeasy Mini kit. Reverse transcription was performed with the Qiagen Quantitect Reverse Transcription kit, which uses random priming and includes a DNase treatment. Resulting cDNA was observed to be free of contaminating gDNA by testing with the mVPA₁ primer set (73). qPCR was performed with BioRad SsoFast EvaGreen master mix on a BioRad CFX96 thermocycler using recommended cycling parameters (hot-start activation at 95°C for 30 s, followed by 40 cycles of 5 s denaturation at 95°C and 5 s annealing/extension at 55°C , followed by melt curve collection from 65 - 95°C in 0.5°C increments at 5 s/step). Inhibition was cleared by diluting samples 1:100 in ddH₂O before analysis. Amplification was confirmed to be target-specific with Primer-BLAST (74) and by observing that melt curves had a single peak consistent with predicted amplicon melting temperature. Primer sequences and target and amplicon details are presented in Supplementary Table A1. Gene-of-interest expression was determined relative to an ensemble of Hprt, Gapdh, and Ldha expression using the GeNorm method (75) implemented by the package eleven (<https://github.com/tdsmith/eleven>).

2.3.5. Mathematical modeling

We constructed mathematical models comprising minimal nonlinear Ordinary Differential Equation (ODE) networks. Network nodes included input signals (LPS+IFN- γ) and (IL-4+IL-13), output markers (CD86 and CD206), and M₁- and M₂-

associated pathways. Model quality was assessed based on optimization of parameters by fitting to the 96-hour timecourse data (Figure 2.2) of four timepoints (24, 48, 72, 96 h) for four different stimulation conditions ($\{0.3,0\}$, $\{0.3,1\}$, $\{0,0\}$, $\{0,1\}$). Parameter optimization was performed using the trust-region-reflective algorithm with the MATLAB optimization toolbox. Model selection was performed using the corrected Akaike Information Criterion (AICc) (76). Details of the mathematical models, optimization, and selection protocol can be found in Appendix A.

3. Effects of extracellular matrix identity, ligand density, and activation on macrophage motility

Migration is an essential function of macrophages. Although monocytes, the circulating precursors to macrophages, are responsible for extravasation and homing to insults, macrophages also live dynamic and motile lives. Macrophage efflux to draining lymph nodes is characteristic of the resolution of inflammation (77). In a more sinister mode, macrophage migration plays a key role in tumor metastasis. Macrophages interact closely with tumor cells to form migrating streams of cells that migrate from the tumor environment into the vasculature, increasing the circulating tumor cell burden (26,27). Defects in macrophage migration can also cause morbidity. For example, the pathogenesis of atherosclerosis is characterized by macrophages which fail to depart fatty plaques (78), and HIV infection can induce migration defects that contribute to pathological accumulation of macrophages in the brain and gut in HIV+ patients (79).

Macrophages acquire a characteristic set of cell adhesion molecules upon differentiation from monocytes (80). Among them are integrins, a family of heterodimeric transmembrane proteins. Integrins function mechanically to anchor cells to their substrata, transduce extracellular signals to intracellular pathways (“outside-in” signaling), and can respond to intracellular signals by changing their affinity for extracellular ligands, mediated through conformation (“inside-out” signaling) (81).

Macrophages express several different integrins with affinity for ECMs including collagen, laminin, and fibronectin. Macrophage integrins are summarized in Table 3.1.

Table 3.1. Mouse BMDM ECM integrins.
 RGD is the peptide motif arginine-glycine-aspartate. Adopted from (82).

α	β	ECM ligand
1	1	Collagen
2		Collagen, laminin
3		Laminin
4		Fibronectin
5		Fibronectin
6		Laminin
M	2	Fibrinogen
V	3	RGD
V	5	RGD

Macrophages depend on integrins for their normal migratory functions. Macrophage efflux from resolving inflammatory environments can be interrupted by blocking integrins with soluble RGD peptides or targeting the $\alpha_4\beta_1$ and $\alpha_5\beta_1$ integrin complexes (83). An accelerated LPS-dependent efflux process depends on the $\alpha_M\beta_2$ integrin (84). Integrins can influence cell function more broadly; when functional integrin signaling was impeded by culturing cells in suspension, applying EDTA to chelate cationic cofactors, or soluble RGD peptides, the intensity of macrophage inflammatory activation was reduced (85). Integrins also play roles in signaling (86).

Studies have assessed the random migration of unstimulated macrophages in 2D as a function of ligand density on fibronectin (87) and the motility and force production of activated macrophages (88). We extend these studies by investigating how activation-

mediated differences in integrin expression are responsible for changes in migratory behavior.

3.1. Results

3.1.1. Macrophage migration velocity decreases with increasing surface fibronectin density

Polydimethylsiloxane (PDMS; Sylgard 184) was used as a receptive substrate for protein adsorption. The amount of rhodamine-fibronectin deposited on a PDMS-coated glass surface increased with the concentration of the coating solution over the range 1-100 $\mu\text{g/ml}$, as detected by fluorescence microscopy of the PDMS surface. The surface begins to saturate between 30 and 100 $\mu\text{g/ml}$ (Supplementary Figure B1).

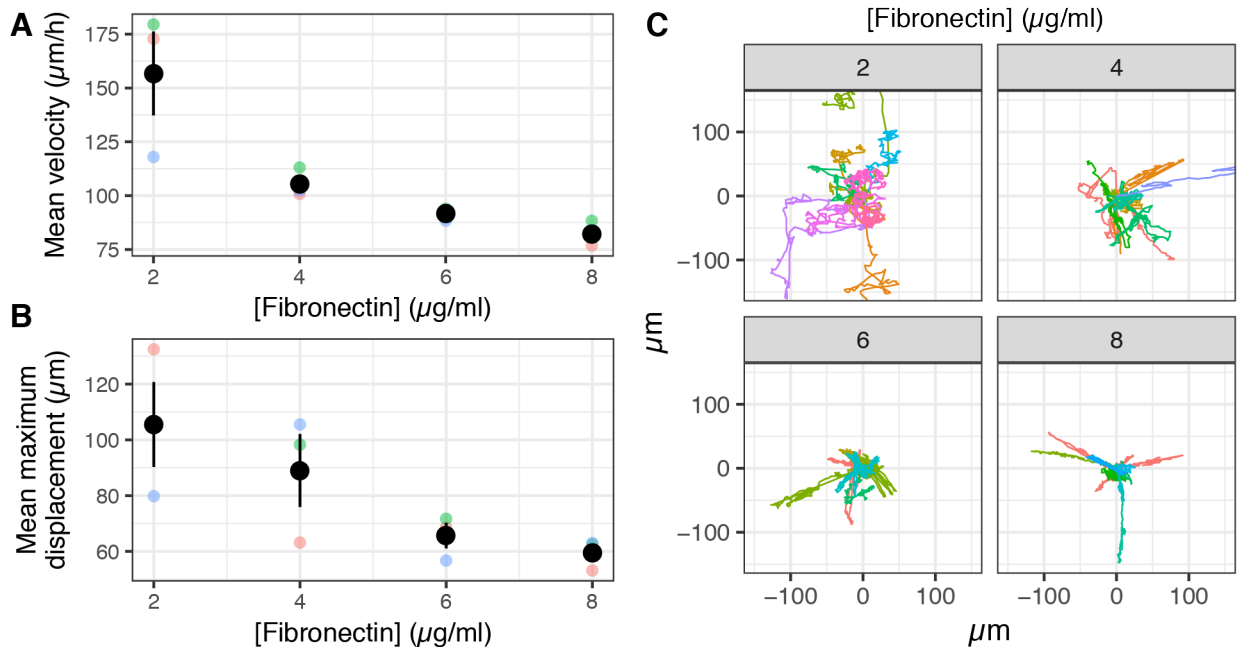


Figure 3.1. Motility of unstimulated macrophages on fibronectin.

A) Migration velocity and B) maximum displacement as a function of fibronectin coating solution concentration. C) Trajectory plots of macrophages migrating on different concentrations of fibronectin, labeled in $\mu\text{g/ml}$. Sampled from Figure 3.3, below.

BMDM were observed migrating on the fibronectin-coated PDMS surfaces for 6 hours.

The migration velocity and average maximum displacement of unstimulated macrophages decreased as the ligand density of fibronectin increased on the surface (Figure 3.1A, B). Macrophages on low densities of fibronectin exhibit erratic trajectories characteristic of a random walk with low persistence. On higher densities of fibronectin, elongated macrophages shuttle back and forth along a linear track (Figure 3.1C).

3.1.2. Macrophage migration velocity has a multiphasic relationship with fibrinogen surface density

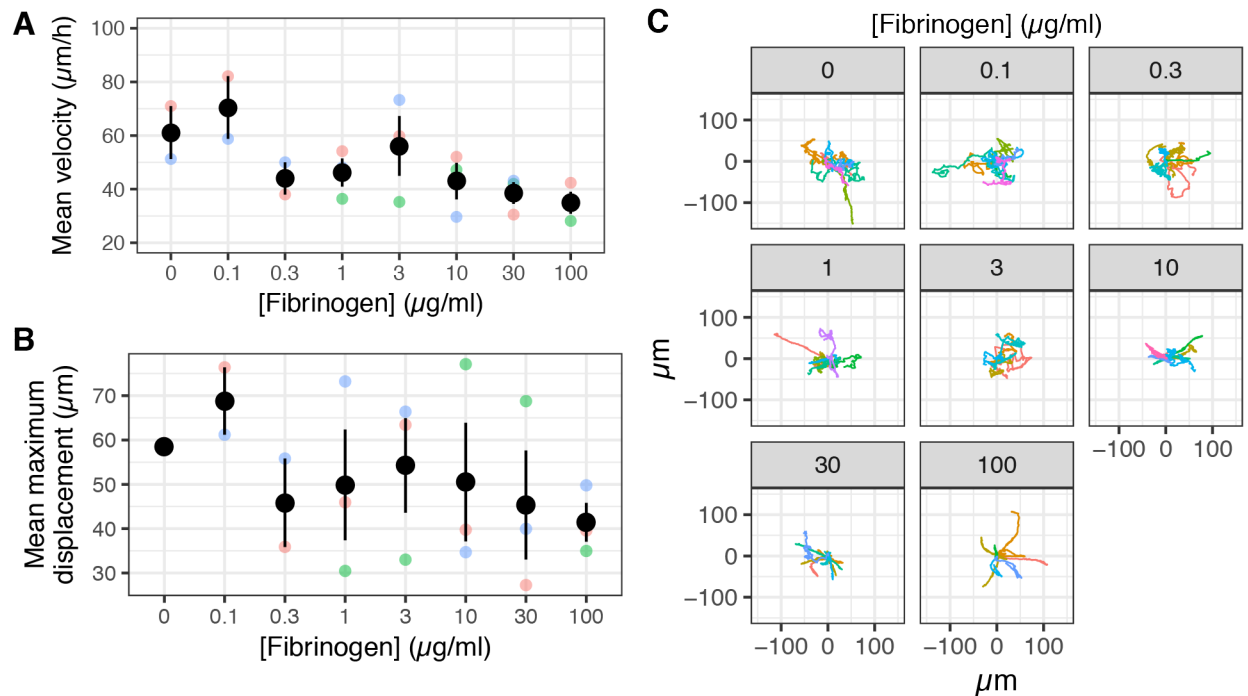


Figure 3.2. Motility of unstimulated macrophages on fibrinogen.

A) Migration velocity and B) maximum displacement as a function of fibrinogen coating solution concentration. C) Trajectory plots of macrophages migrating on different concentrations of fibrinogen, labeled in $\mu\text{g/ml}$.

On fibrinogen, macrophage migration velocity as a function of ligand density resembles the classic multiphasic relationship described by DiMilla, Barbee, and Lauffenburger (89) (Figure 3.3A). At very low ligand densities, macrophages interact with the surface weakly. Near $0.3 \mu\text{g/ml}$, macrophage migration velocity decreases, as macrophages begin to

interact with the surface but are unable to generate significant force. Macrophage migration peaks near 3 $\mu\text{g}/\text{ml}$, where force production and adhesive forces balance. Migration velocity decreases with further increasing concentration as adhesive forces dominate the surface interaction. At high ligand densities, macrophages on fibrinogen display the same linear migration behavior as macrophages on fibronectin (Figure 3.3B).

3.1.3. M1 polarization slows macrophage migration on fibronectin and fibrinogen

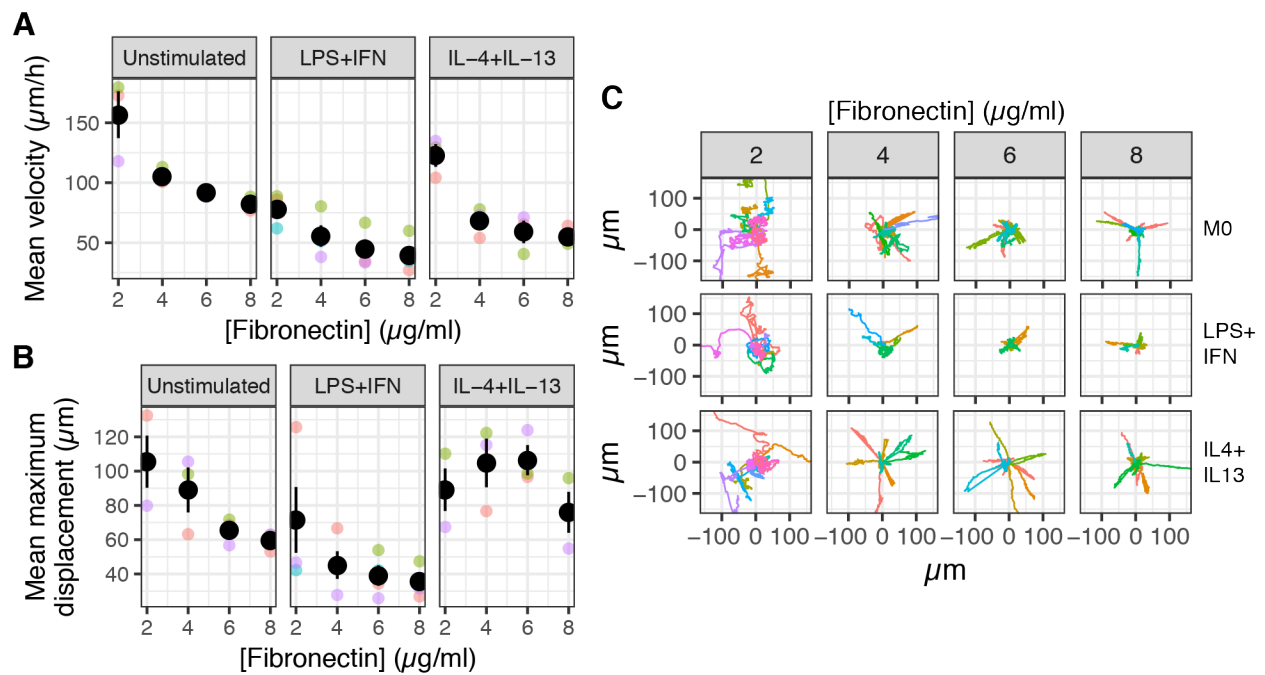


Figure 3.3. Combined effects of activation and fibronectin ligand density on macrophage migration.

A) BMDM migration velocity, B) maximum displacement, and C) representative ($n=10$) trajectory plots of moving cells as a function of fibronectin concentration and macrophage polarization.

On fibronectin, macrophage migration was slowed by LPS+IFN- γ treatment (Figure 3.3A).

LPS+IFN- γ -treated macrophages were less likely to migrate far from their starting position. On low ligand densities, macrophage migration appeared qualitatively random, regardless of activation (Figure 3.3B). IL-4+IL-13-treated macrophages migrated in linear

tracks at intermediate ligand densities, while unstimulated macrophages still retained a more random migratory pattern.

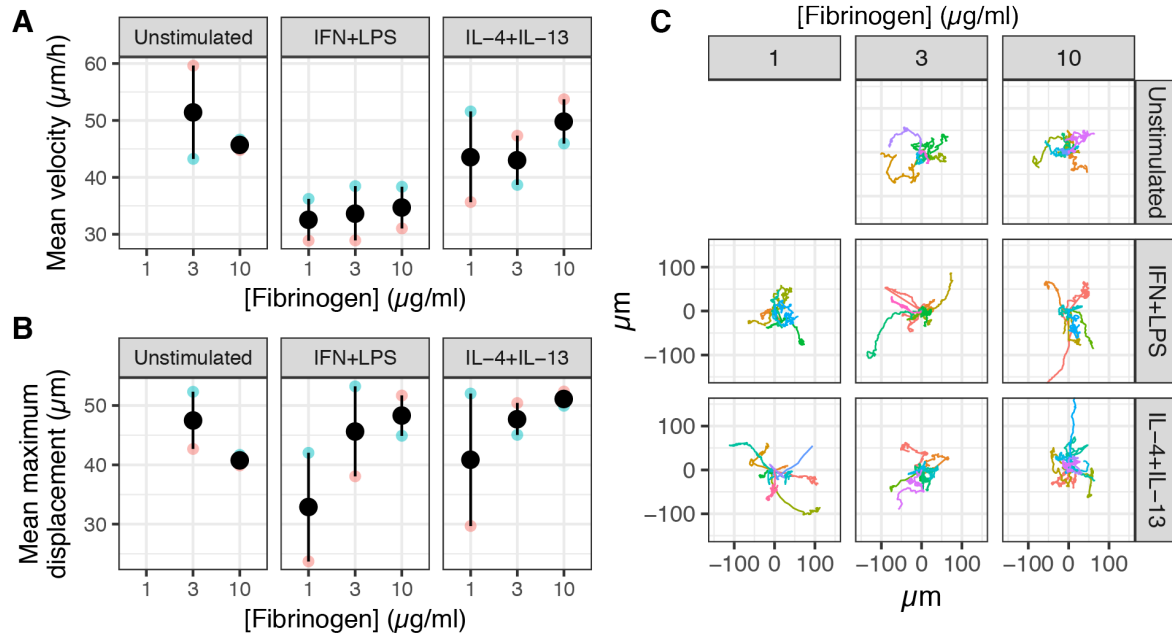


Figure 3.4. Combined effects of activation and fibrinogen ligand density on macrophage migration. A) BMDM migration velocity, B) maximum displacement, and C) representative ($n=10$) trajectory plots of moving cells as a function of fibrinogen concentration and macrophage polarization.

LPS+IFN- γ activation also slowed cells on fibrinogen (Figure 3.4A). Migration on fibrinogen was, in general, slower than migration on fibronectin. Unlike cells on fibronectin, cells on fibrinogen did not display any increased tendency towards more linear migration after cytokine stimulation (Figure 3.4C).

3.1.4. Macrophage polarization drives differential integrin expression

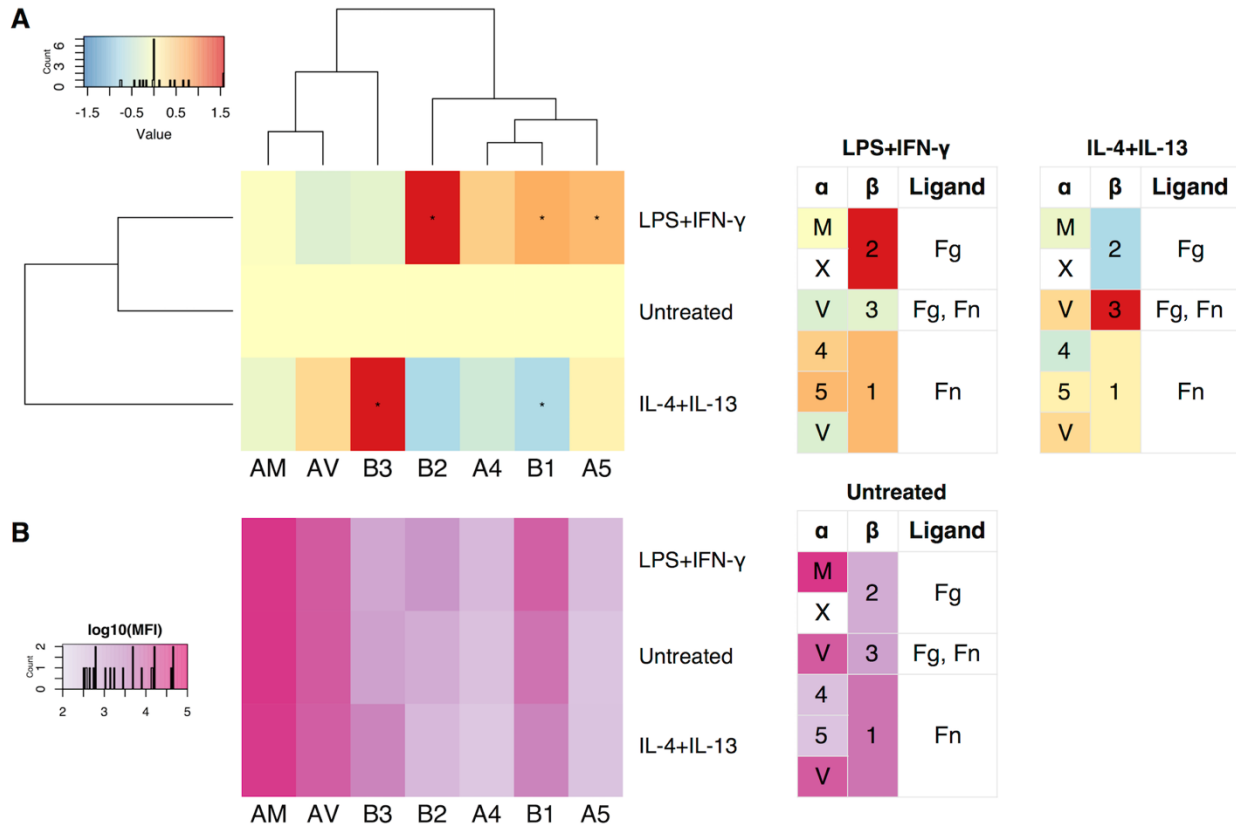


Figure 3.5. Integrin expression changes 24 h after macrophage activation.

A) Median fluorescence intensity of flow cytometry data, expressed as \log_2 fold expression vs untreated macrophages. The colors from the heat map are mapped on to Table 3.1 to relate integrin expression to expected matrix affinities. Asterisks indicate significant differences vs unstimulated by pairwise t-test, FDR < 0.05. B) \log_{10} absolute value of median fluorescence intensity of flow cytometry data for integrins, to illustrate approximate relative abundance.

We proposed that activation-driven changes in integrin expression could be responsible for changes we observed in migratory behavior and assessed integrin expression by flow cytometry. LPS+IFN- γ treatment increased the surface expression of α_5 , β_1 , and β_2 integrins, which is consistent with higher affinity for both fibrinogen and fibronectin (Figure 3.5A). Expression of α_V and β_3 integrin was slightly reduced. IL-4+IL-13-stimulated macrophages showed a substantially opposite trend, with increased surface expression of the RGD-binding β_3 integrin, sensitive to both fibronectin and fibrinogen, and lower expression of the β_1 integrin. All flow cytometry histograms were essentially unimodal, so

changes in median fluorescence intensity (MFI) are a useful description of the integrin expression of the cell population (Supplementary Figure B2). Absolute MFI after multicolor compensation was plotted to give an approximate indication of integrin abundance (Figure 3.5B) since isotype staining intensity was similar in each condition. As expected for macrophages, α_M integrin is highly expressed; the α_M integrin showed relatively little variation between activation conditions. The α_4 and α_5 integrins had lower expression.

3.1.5. Blockade of $\alpha_V\beta_3$ integrin has minimal effects on migration

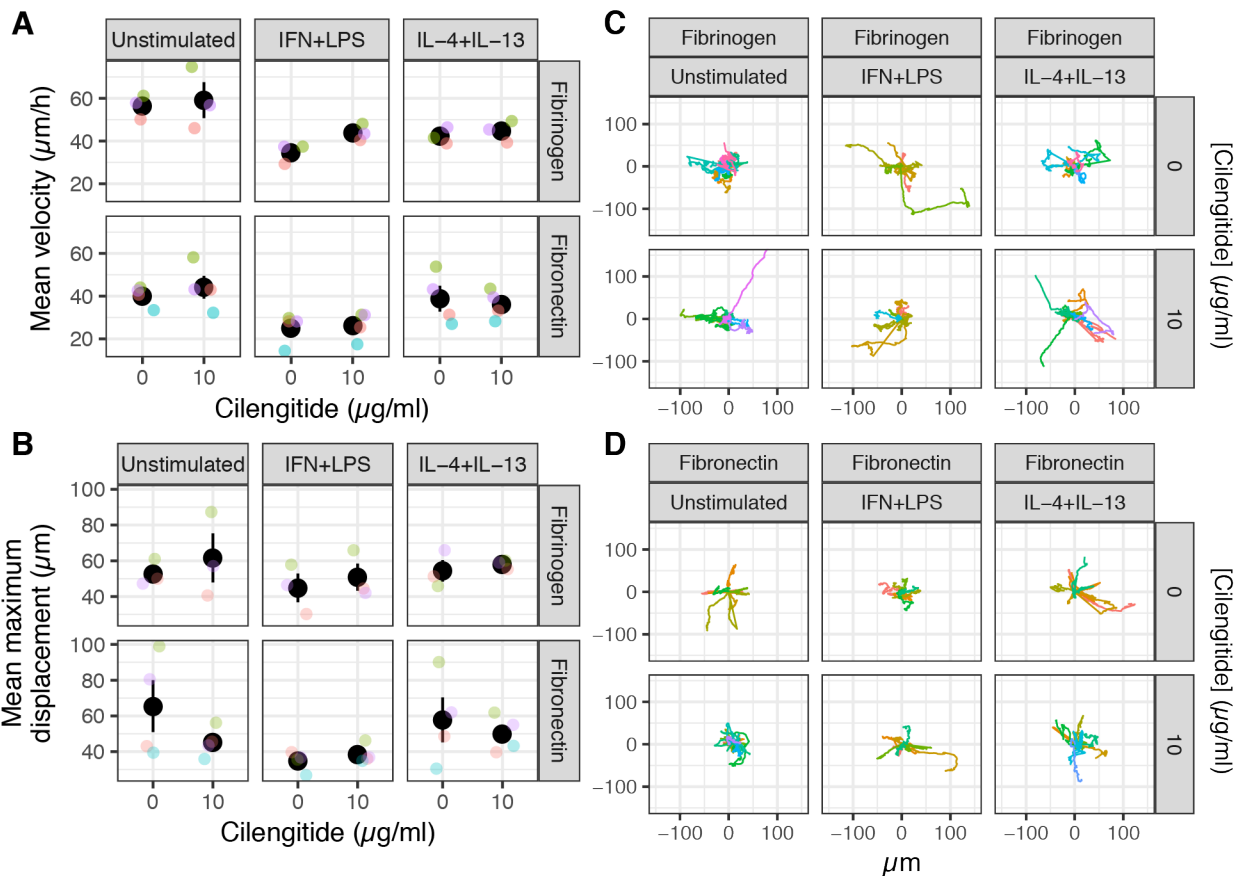


Figure 3.6. Effects of cilengitide on macrophage migration.

A) Mean velocity of BMDM migrating on fibrinogen and fibronectin surfaces with or without cilengitide treatment. B) Mean maximum displacement from the origin. C) Representative trajectory plots of BMDM (n=10) on fibrinogen. D) Representative trajectory plots of BMDM (n=10) on fibronectin.

Cilengitide is a cyclic RGD pentapeptide with blocking activity against the RGD-binding $\alpha_v\beta_3$ and $\alpha_v\beta_5$ integrins (90). Expression of β_3 integrin was highest on IL-4+IL-13-treated macrophages and modestly lower on LPS+IFN- γ -treated macrophages. On fibronectin and fibrinogen surfaces coated with 3 $\mu\text{g/ml}$ ECM solutions, cilengitide treatment had a modest effect on the average maximum displacement of unstimulated macrophages (Figure 3.6B), which could indicate a less persistent migratory mode. Migration velocity was not affected (Figure 3.6A) and trajectories were otherwise qualitatively similar (Figure 3.6C-D).

3.1.6. Antibody blockade of β integrins has minimal effects on migration

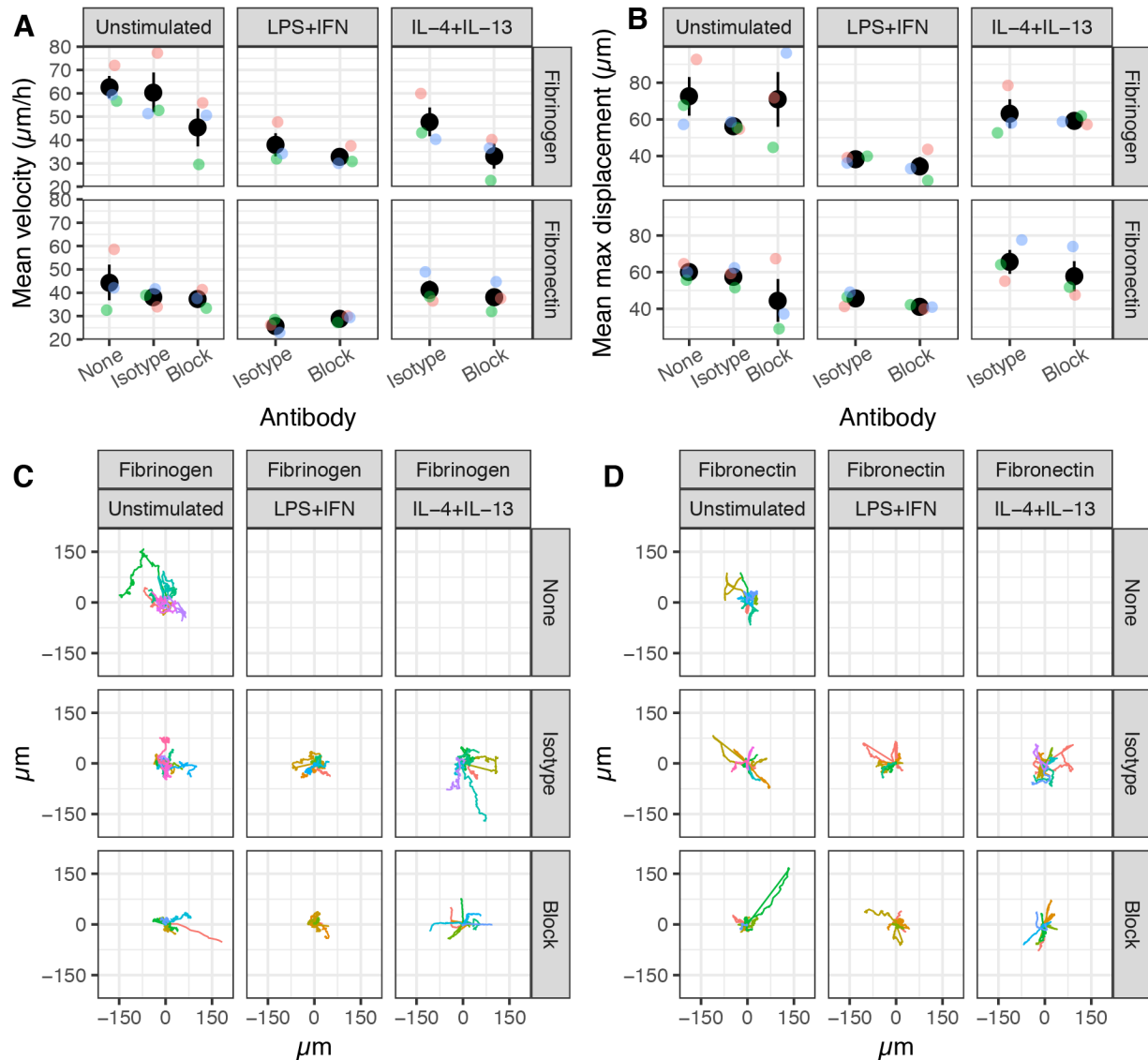


Figure 3.7. Effects of antibody blockade on macrophage migration.

A) Mean velocity and B) mean maximum displacement of BMDM trajectories. C) Representative trajectories of BMDM (n=10) on fibronectin. D) Representative trajectories of BMDM (n=10) on fibrinogen.

We tested the ability of a cocktail of anti- β -integrin antibodies targeting the β_1 , β_2 , and β_3 integrin chains to disrupt cell-matrix interactions by assessing macrophage motility.

There were no significant differences in migration velocity (Figure 3.7A) although 2 of 3 biological replicates indicated a non-significant decrease in the velocity of unstimulated or IL-4+IL-13-treated macrophages on fibrinogen. There was also a non-significant

decrease in maximum attained displacement in the unstimulated condition on fibronectin (Figure 3.7B).

3.1.7. siRNA-mediated knockdown of integrins affects motility and changes cell shape

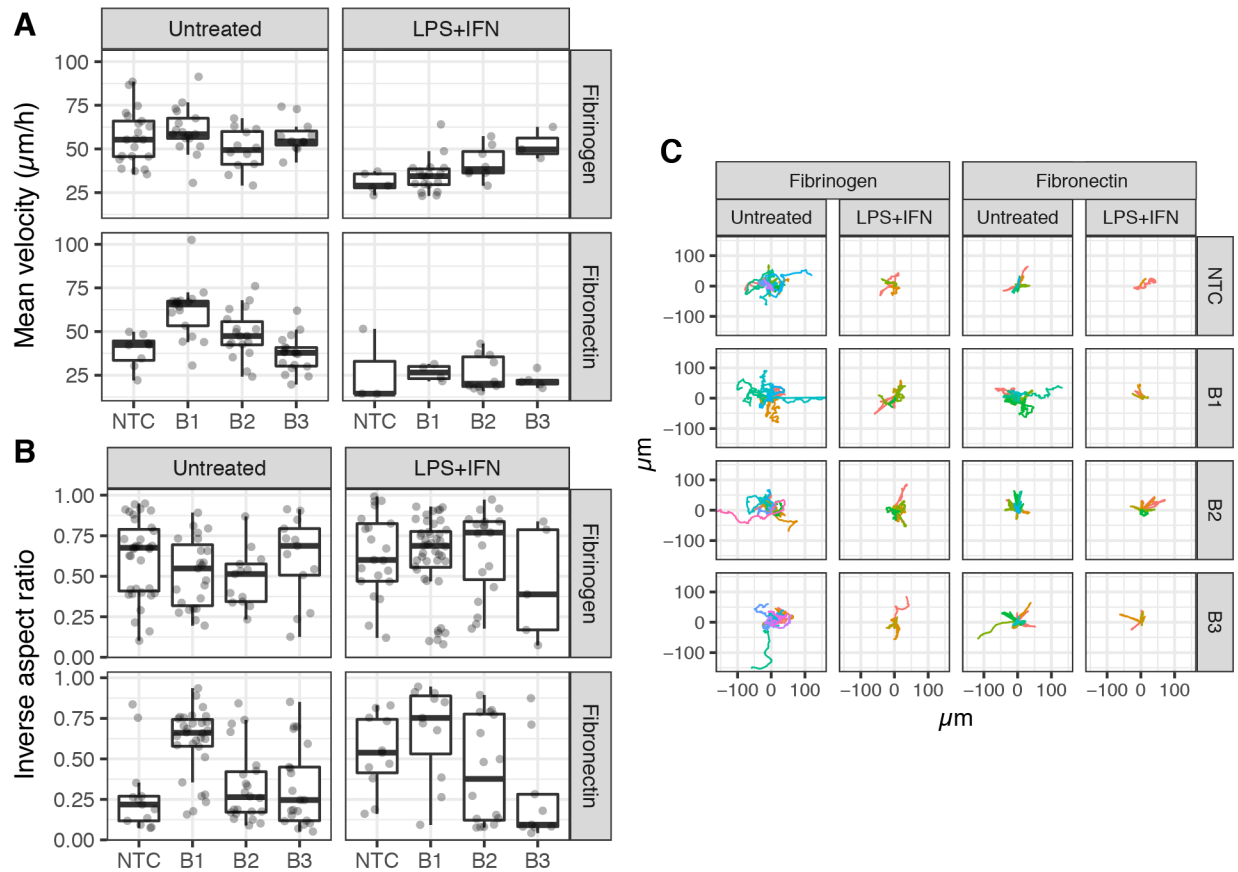


Figure 3.8. Effect of siRNA-mediated integrin knockdown on macrophage motility and shape. A) Mean velocity of BMDM. B) Inverse aspect ratio of BMDM. c) Representative trajectories of cells (n=10) migrating on fibrinogen and fibronectin after integrin knockdown.

We performed a pilot experiment to assess the ability of siRNA-mediated knockdown to modify macrophage migration behaviors. After demonstrating successful knockdown by Western blot (data not shown), motility was observed. On fibronectin, disrupting β_1 integrin activity increased the speed of unstimulated cells (Figure 3.8A) and caused macrophages to adopt a rounder shape with and without LPS+IFN- γ treatment (Figure

3.8B). The trajectories of the unstimulated β_1^{KO} cells appeared more random than controls (Figure 3.8C). Interestingly, in contrast to the NTC control, the velocity of cells in the β_3 integrin KO condition on fibrinogen was not affected by LPS+IFN- γ treatment, although the number of cells that were available for analysis was small. Cells in the β_3^{KO} LPS+IFN- γ condition were also elongated.

3.2. Discussion

We confirm results from recent studies that macrophage migration depends on polarization and the area density of ECM ligands. We additionally observe distinct random and linear migration modes as a function of fibronectin, but not fibrinogen, ligand density. Macrophage activation is found to provoke changes in the surface expression of integrins. In the case of LPS+IFN- γ treatment, the integrin expression pattern favors greater adhesion to fibrinogen and fibronectin; in the case of IL-4+IL-13 treatment, expression of the RGD-binding β_3 integrin is favored. Cilengitide had a modest effect on the track persistence of unstimulated macrophages; an anti- β -integrin antibody blockade did not effectively interrupt ligand-matrix interactions. A siRNA-mediated knockdown experiment demonstrated control of adhesion to fibronectin.

The relationship between migration velocity and fibronectin density did not resemble the classical biphasic distribution predicted by modeling (89) and recently observed in RAW 264.7 macrophages (87). In the latter study, macrophage trajectories did not resemble the linear migration tracks that we observed here on fibronectin and that we and other commenters (91) have observed incidentally on glass (data not shown), where serum vitronectin is the dominant adhesive intermediary (92). Notably, the shift to linear

migration tracks from random tracks occurred at a lower matrix density in the IL-4+IL-13-treated case, which resulted in increased β_3 integrin expression, and vitronectin is a β_3 integrin ligand, which suggests the possibility that the linear migration behavior requires a sufficient degree of β_3 -mediated adhesion. Further work could examine whether siRNA-mediated β_3 knockdown changes the BMDM preference for the linear migration mode on glass and fibronectin surfaces, or whether the β_3 inhibitor cilengitide affects the threshold ligand density for random-dominant vs. linear-dominant trajectories.

Another possibility is suggested by the finding that, in fibroblasts and epithelial cells, increased Rac1 activity was associated with a greater degree of random, versus persistent, migration; suppressing Rac1 led to enhanced directional persistence (93). Some information about the regulation of macrophage migration has been derived using biochemical inhibitors; for example, random migration of unstimulated RAW 264.7 macrophages depends absolutely on PI3K, is independent of Cdc42, and is reduced by ROCK inhibition on high ligand densities (87). Assessing Rac1 activity with a reporter assay could also shed light on the hypothesis that the linear migration behavior we observed is Rac1-dependent. Reporter assays are more technically challenging than pharmacological inhibition but severe off-target effects have been reported for the most popular small-molecule Rac1 inhibitors (94,95).

Macrophage activation is linked to migration through several interacting factors of different weights. Null results do not exclude the possibility of integrin mediation but may place a limit on its influence. For instance, BMDM from mice deficient for the M2

marker CD206 exhibit faster random migration on glass coverslips relative to WT BMDM, by an undetermined mechanism (96). In Chapter 2, it was demonstrated that LPS+IFN- γ treatment downregulates CD206, yet LPS+IFN- γ -treated macrophages clearly migrate more slowly overall. As well, there may be a dynamic relationship between macrophage migration and integrin expression. RhoB^{-/-} macrophages have similar expression of β_1 integrins and reduced expression of β_2 and β_3 integrins compared to WT BMDM (97); since mechanical tension can activate Rho GTPases, this suggests that integrin-derived feedback may regulate integrin expression in macrophages, which could complicate integrin-blocking assays.

The statistical treatment of migration data poses thorny questions. Random migration is a fundamentally stochastic process wherein individual cells exposed to nominally identical conditions behave differently. Because the variation between cells is large, it is necessary to observe a large number of cells to confidently describe the population within each biological replicate. Because BMDMs resist labeling with nuclear stains, tracking cells is laborious. Primary cells also exhibit biological variation between mice. This work has adopted the practice of averaging the measurements of all cells observed from a single mouse and treating the 3 or 4 resulting means for each parameter as independent observations, i.e. the basis of n . Although this approach is principled, it is not very powerful, in the sense that a larger basis of observations is probably necessary to permit statistical resolution of differences on the scale we observed.

Another challenge is parameterizing migration trajectories. Random-walk models are often used to describe cell motility (98), including of macrophages (87,88), and we

explored applying random-walk models to the data we collected. Our experience was that the random-walk models did not contribute information that was not accessible from the velocity and displacement parameters. The random-walk models do not naturally represent the kind of linearly directed back-and-forth migration that we observed in several conditions, which undercuts the utility of and theoretical basis for their application. Random-walk models have been rejected for migration in 3D contexts (99) in favor of models incorporating an explicit treatment of cellular heterogeneity, and anisotropic speed and self-correlation terms (100). Applying a more sophisticated model could allow us to more finely parse the differences we can observe by eye in macrophage migration trajectory plots although the intrinsic stochasticity of migration may not permit an accurate estimation of additional parameters.

Direct measurement of cell adhesion strength, as by a spinning disk (101), micropipette aspiration, or timed exposure assay could provide interesting adjunct information about the interactions between macrophages and the substrate that could support an interpretation of the integrin blockade and knockout experiments.

Regulating macrophage migration has been proposed as a therapeutic avenue (102). In fact, the small molecule anti-inflammatory drug pirfenidone works in part by interrupting macrophage chemotaxis (103). Polymers eluting a RGD-blocking peptide resulted in a thinner capsule in WT mice than control polymers (104). This study supports the principle that macrophage phenotype is linked to adhesion and motility.

3.3. Methods

3.3.1. Cell culture

BMDM were prepared and used as described in Chapter 2. Lyophilized fibrinogen (Sigma) was prepared to a stock concentration of 2 mg/ml, passed through a 0.2 μ m filter, and stored at -20 °C until use. Fibronectin (Corning) was prepared to a stock concentration of 1 mg/ml following manufacturer's directions and stored at -20 °C until use. Cilengitide (Tocris) was used at a concentration of 10 μ g/ml. Antibodies were used at a concentration of 10 μ g/ml each.

3.3.2. Random migration

8-well chamber slides (Thermo Scientific Lab-Tek II) were coated with a thin layer of 9:1 Sylgard 184 (Dow Corning) PDMS:crosslinker and cured at 60 °C overnight. PDMS surfaces were rendered hydrophilic by UV/ozone treatment for 8 minutes (105). Protein solution was applied in PBS for 1 hour at room temperature, rinsed thoroughly with PBS, and replaced by 0.2% Pluronic F-127 in PBS for an additional hour to block remaining exposed PDMS. After additional rinsing, 2,000 cells were seeded in each well. Cytokines and/or integrin-blocking agents were applied at 24 hours after seeding and slides were observed for 6 hours at 2 minute intervals at 48 hours after seeding. Chambers were observed with an Olympus IX-83 inverted microscope equipped with a Tokai Hit stage incubator and controlled by Micro-Manager. Incubator settings were chosen to maintain cells at 37 °C, as measured by a thermoresistive probe, in a 5% CO₂ atmosphere. At least three fields of view were sampled in each well of the chamber slide.

Nuclear tracking dyes commonly used for live cell imaging, including Hoechst 33342, DRAQ5, and CyTrak Orange, were rapidly toxic to BMDM and could not be used. The centers of cell nuclei were annotated by hand using MTrackJ (106). Cells migrating fewer than 20 μm from their origin were considered non-moving and were excluded from analyses.

3.3.3. Antibodies

For flow cytometry, antibodies against α_{M} (M1/70 PE), α_{V} (RMV-7 PE), β_2 (M18/2 FITC), and β_3 (2C9.G2 APC) integrins were from Biolegend. PE-conjugated antibodies against α_4 , α_5 , and β_1 integrins were from Santa Cruz Biotechnology. Isotype controls were purchased from the corresponding vendor. Fc block antibody was from Tonbo. For blocking, LEAF-grade antibodies against β_1 (HM β_1 -1), β_2 (M18/2), and β_3 (2C9.G2) integrins and matching isotype controls were purchased from Biolegend.

3.3.4. siRNA

Day 7 BMDM were transformed with the Lonza 4D-Nucleofector system using proprietary primary solution 3, supplement 1, and program DS-137. siGENOME siRNAs were ordered for each target gene from Dharmacon. After transformation, cells were maintained in RPMI 1640 supplemented with 10% supernatant from Ltk- cells secreting recombinant mouse MCSF and 10% heat-inactivated FBS.

4. Conclusions and future directions

The studies described in this work investigate how macrophages integrate and respond to signals in their microenvironment. Chapter 2 presented an *in vitro* model of macrophages displaying markers for both M₁ and M₂ activation, demonstrated that these mixed macrophage phenotypes can arise as a response to simultaneous presentation of activation signals, and showed that costimulated macrophages shift from a M₁-dominant to a M₂-dominant presentation over time. Chapter 3 explored how macrophage activation and surface ligand density conspire to influence macrophage motility and revealed that this interaction is different on fibrinogen, which is abundantly displayed on biomaterial surfaces and in the early stages of wound healing, and fibronectin, which is an important constituent of the provisional matrix that forms in the middle stages of wound healing. Both studies underscore the plastic nature of macrophage response to their environment.

Extending our studies of migrating macrophages to 3D matrices would represent a natural progression. Macrophages are known to migrate through 3D matrices in ways that depend on macrophage phenotype and the properties of the matrix. Macrophages in 3D use both adhesion-dependent mesenchymal cell migration mode and adhesion-independent amoeboid migration mode depending on the structure of the local ECM (107). These migratory behaviors are known to be influenced by macrophage activation; M₂ macrophages showed enhanced abilities to penetrate and degrade dense matrices compared to unactivated macrophages or cells of different lineages (108).

Models of wound matrix are an interesting system where migration has not been characterized.

The understanding that different modes of macrophage activation confer different abilities to degrade and remodel extracellular matrices also offers a basis for developing the results of the migration study. A pilot experiment we performed on surfaces coated with fluorescent fibronectin revealed cell-associated dark spots presumably related to cell-mediated degradation of the matrix. Assessing ECM monolayer degradation as a function of ligand density or adapting this assay to a format suitable for live-cell imaging could reveal whether the patterns we observed in macrophage migration trajectories can be explained by matrix remodeling. In particular, it could explain the tendency for cells to shuttle back and forth or double back on their tracks.

Studies of macrophage migration can also proceed to higher or lower length scales. Macrophage adhesion is unusual in that it is mediated by podosomes, which are similar to but distinct from focal adhesions; they are characteristically smaller and shorter-lived than focal adhesions (109). Focal adhesions are the primary sites of integrin-matrix contact and are indispensable for migration in most cell types. Macrophages, however, have been observed to migrate even after podosome formation was abolished (91). Understanding how cell-matrix adhesion is organized and regulated during migration and how activation alters podosome formation could add an important dimension to this work. At the higher length scale, studies of collective migration are of interest. Macrophage interactions with tumor cells leading to streaming migration towards the circulation may be an important event in metastasis (27,28). Understanding how

activation affects these interactions and how to disrupt them could lead to a better understanding of metastasis and how to interrupt it.

Development of alternative models for quantifying migration could help present the trends evident in the geometric but not the scalar descriptions of migration trajectories. These metrics could be as simple as a descriptive measure of the linearity of the cell position point clouds or as complex as introducing new formalisms to explore underlying mechanisms (110).

The activation study in Chapter 2 and the migration study in Chapter 3 employed different methods of assessing macrophage behavior. The activation study reflected a marker-based approach to macrophage phenotyping. Many markers are easy to detect but have uncertain or untranslatable biological effects. Classifying mouse macrophages on the basis of arginase I expression is an example; *Arg1* transcript levels in mouse BMDM change more than 1,000-fold upon IL-4 stimulation, but, while *Arg1* expression in mice is linked to regulation of nitric oxide synthesis (111) and has a speculative association with matrix synthesis (112), *Arg1* is not expressed in human macrophages at all. Nonetheless, *Arg1* expression at the transcript or protein levels is conveniently and inexpensively assayed and, because the products of macrophage activation are generally co-regulated, can predict mouse macrophage function. The majority of work on macrophage activation relies on markers. Conversely, functional studies can observe behaviors like migration, giant cell formation, and phagocytosis directly related to macrophage-driven outcomes, which lends a stronger sense that the assays measure something biologically important. Functional assays are often more laborious to perform, difficult to multiplex, and more

subtle to quantify. Cytokine secretion is something of a middle ground, in that cytokine secretion is straightforward to detect and part of the functional role of the macrophage.

Recent work has highlighted that it is possible to use omics approaches to parse macrophage responses to stimuli more finely (e.g., (11)). These studies necessarily function at the marker level. While the straightforward M₁-M₂ paradigm is useful because it concisely reflects observable and, importantly, druggable (113), differences in cell behavior, characterizing macrophages in wound and tumor models with higher-dimensional models may shed light on how the response of macrophages is modulated by the additional factors present in pathological environments. Indeed, a complementary opportunity is to characterize macrophage behavior under more complex activation conditions. Tumor cell line coculture models provide a less reductionist but still accessible approach for evaluating how the tumor environment influences immune behavior (114-117). Models for assessing macrophage migration in the context of tumor spheroids have also been proposed (118). Using decellularized organ slurries as components of an *in vitro* study of the effects of matrix components on macrophage phenotype has also been explored (119). Of course, the challenge of recapitulating a physiological environment is to ensure that the greater specificity of the experimental system actually contributes greater realism and not just different artefacts. Recent progress in efficiently isolating tissue macrophages and tumor-associated macrophages offers the promise of being able to examine macrophages in a genuinely physiological context (120,121).

The work in chapter 3 reflects progress towards demonstrating that changes in cell-surface integrin expression driven by activation can influence migration. Ongoing studies in the lab are examining the effects of siRNA-mediated integrin knockdown on macrophage activation responses; integrins are required for some signaling responses and pattern recognition in macrophages (86). The migration assays developed for this work describe a functional property of macrophages and will naturally complement our marker-based assessments.

The evolution of macrophage phenotypes over time, as observed in wound healing and in the response to implanted materials, and the migration of macrophages in response to activation and their substrata represent fundamental processes of these versatile and powerful cells. There are opportunities to translate these findings towards the clinic. Integrin-targeted therapies have been proposed to help control the macrophage foreign body response to materials (104,122) and finding ways to interrupt tumor-associated macrophage migration could lead to therapeutic breakthroughs in cancer treatment. With further study, deeper understanding of these processes should lead to finer control of macrophage responses to improve human health.

References

1. Häggström M, Rad A. Hematopoiesis [Internet]. 2016. Available from: https://commons.wikimedia.org/wiki/File:Hematopoiesis_simple.svg
2. Riley LK, Rupert J. Evaluation of Patients with Leukocytosis. *Am Fam Physician*. 2015 Dec 1;92(11):1004–11.
3. Epelman S, Lavine KJ, Randolph GJ. Origin and Functions of Tissue Macrophages. *Immunity*. 2014 Jul;41(1):21–35.
4. Franklin RA, Li MO. Ontogeny of Tumor-Associated Macrophages and Its Implication in Cancer Regulation. *Trends in Cancer*. 2016 Jan;2(1):20–34.
5. Dalton D, Pitts-Meek S, Keshav S, Figari I, Bradley A, Stewart T. Multiple defects of immune cell function in mice with disrupted interferon-gamma genes. *Science*. 1993 Mar 19;259(5102):1739–42.
6. Mosser DM, Edwards JP. Exploring the full spectrum of macrophage activation. *Nat Rev Immunol*. 2008 Dec;8(12):958–69.
7. Alfonso-García A, Smith TD, Datta R, Luu TU, Gratton E, Potma EO, et al. Label-free identification of macrophage phenotype by fluorescence lifetime imaging microscopy. *Journal of Biomedical Optics*. 2016 Apr 18;21(4):46005.
8. McWhorter FY, Wang T, Nguyen P, Chung T, Liu WF. Modulation of macrophage phenotype by cell shape. *Proceedings of the National Academy of Sciences*. 2013 Oct 22;110(43):17253–8.
9. Kadl A, Meher AK, Sharma PR, Lee MY, Doran AC, Johnstone SR, et al. Identification of a novel macrophage phenotype that develops in response to atherogenic phospholipids via Nrf2. *Circ Res*. 2010 Sep 17;107(6):737–46.
10. Martinez FO, Gordon S. The M1 and M2 paradigm of macrophage activation: time for reassessment. *F1000Prime Reports* [Internet]. 2014 Mar 3 [cited 2017 Feb 13];6. Available from: <http://www.f1000.com/prime/reports/b/6/13>
11. Xue J, Schmidt SV, Sander J, Draffehn A, Krebs W, Quester I, et al. Transcriptome-based network analysis reveals a spectrum model of human macrophage activation. *Immunity*. 2014 Feb 20;40(2):274–88.
12. Mirza R, DiPietro LA, Koh TJ. Selective and specific macrophage ablation is detrimental to wound healing in mice. *Am J Pathol*. 2009 Dec;175(6):2454–62.

13. Lucas T, Waisman A, Ranjan R, Roes J, Krieg T, Muller W, et al. Differential Roles of Macrophages in Diverse Phases of Skin Repair. *J Immunol*. 2010 Apr 1;184(7):3964–77.
14. Koh TJ, DiPietro LA. Inflammation and wound healing: the role of the macrophage. *Expert Rev Mol Med*. 2011 Jul 11;13:e23.
15. Martin P, Nunan R. Cellular and molecular mechanisms of repair in acute and chronic wound healing. *British Journal of Dermatology*. 2015 Aug;173(2):370–8.
16. Sindrilaru A, Peters T, Wieschalka S, Baican C, Baican A, Peter H, et al. An unrestrained proinflammatory M1 macrophage population induced by iron impairs wound healing in humans and mice. *J Clin Invest*. 2011 Mar;121(3):985–97.
17. Satoh T, Kidoya H, Naito H, Yamamoto M, Takemura N, Nakagawa K, et al. Critical role of Trib1 in differentiation of tissue-resident M2-like macrophages. *Nature*. 2013 Mar 28;495(7442):524–8.
18. Shiraishi M, Shintani Y, Shintani Y, Ishida H, Saba R, Yamaguchi A, et al. Alternatively activated macrophages determine repair of the infarcted adult murine heart. *J Clin Invest*. 2016 Jun 1;126(6):2151–66.
19. Zhu Z, Ding J, Ma Z, Iwashina T, Tredget EE. Systemic depletion of macrophages in the subacute phase of wound healing reduces hypertrophic scar formation. *Wound Repair Regen*. 2016 Jul;24(4):644–56.
20. Pollard JW. Tumour-educated macrophages promote tumour progression and metastasis. *Nat Rev Cancer*. 2004 Jan;4(1):71–8.
21. Mantovani A, Sozzani S, Locati M, Allavena P, Sica A. Macrophage polarization: tumor-associated macrophages as a paradigm for polarized M2 mononuclear phagocytes. *Trends in Immunology*. 2002 Nov 1;23(11):549–55.
22. Guo X, Zhao Y, Yan H, Yang Y, Shen S, Dai X, et al. Single tumor-initiating cells evade immune clearance by recruiting type II macrophages. *Genes & Development*. 2017 Feb 1;31(3):247–59.
23. Solinas G, Germano G, Mantovani A, Allavena P. Tumor-associated macrophages (TAM) as major players of the cancer-related inflammation. *J Leukocyte Biol*. 2009 Nov 1;86(5):1065–73.
24. Condeelis J, Pollard JW. Macrophages: Obligate Partners for Tumor Cell Migration, Invasion, and Metastasis. *Cell*. 2006 Jan;124(2):263–6.
25. Guet R, Van Goethem E, Cougoule C, Balor S, Valette A, Al Saati T, et al. The process of macrophage migration promotes matrix metalloproteinase-independent invasion by tumor cells. *J Immunol*. 2011 Oct 1;187(7):3806–14.

26. Wyckoff JB, Wang Y, Lin EY, Li J -f., Goswami S, Stanley ER, et al. Direct Visualization of Macrophage-Assisted Tumor Cell Intravasation in Mammary Tumors. *Cancer Research*. 2007 Mar 15;67(6):2649–56.
27. Patsialou A, Bravo-Cordero JJ, Wang Y, Entenberg D, Liu H, Clarke M, et al. Intravital multiphoton imaging reveals multicellular streaming as a crucial component of in vivo cell migration in human breast tumors. *IntraVital*. 2013 Apr;2(2):e25294.
28. Sharma V, Beaty BT, John S, Robert J. Reconstitution of in vivo macrophage-tumor cell pairing and streaming motility on one-dimensional micro-patterned substrates. 2012;(September):77–85.
29. Anderson JM, Rodriguez A, Chang DT. Foreign body reaction to biomaterials. *Seminars in Immunology*. 2008 Apr;20(2):86–100.
30. Coleman DL, King RN, Andrade JD. The foreign body reaction: A chronic inflammatory response. *Journal of Biomedical Materials Research*. 1974 Sep;8(5):199–211.
31. Biswas SK, Mantovani A. Macrophage plasticity and interaction with lymphocyte subsets: cancer as a paradigm. *Nat Immunol*. 2010 Oct;11(10):889–96.
32. Mills CD, Kincaid K, Alt JM, Heilman MJ, Hill AM. M-1/M-2 Macrophages and the Th1/Th2 Paradigm. *J Immunol*. 2000 Jun 15;164(12):6166–73.
33. Anderson JM, Rodriguez A, Chang DT. Foreign body reaction to biomaterials. *Semin Immunol*. 2008 Apr;20(2):86–100.
34. Martinez FO, Gordon S. The M1 and M2 paradigm of macrophage activation: time for reassessment. *F1000Prime Reports*. 2014 Jan;6(March):13.
35. Ohmori Y, Hamilton TA. IL-4-induced STAT6 suppresses IFN-gamma-stimulated STAT1-dependent transcription in mouse macrophages. *J Immunol*. 1997 Dec 1;159(11):5474–82.
36. Venkataraman C, Leung S, Salvekar A, Mano H, Schindler U. Repression of IL-4-induced gene expression by IFN-gamma requires Stat1 activation. *J Immunol*. 1999 Apr 1;162(7):4053–61.
37. te Velde AA, de Waal Malefijt R, Huijbens RJ, de Vries JE, Figdor CG. IL-10 stimulates monocyte Fc gamma R surface expression and cytotoxic activity. Distinct regulation of antibody-dependent cellular cytotoxicity by IFN-gamma, IL-4, and IL-10. *J Immunol*. 1992 Dec 15;149(12):4048–52.

38. Stöger JL, Gijbels MJJ, van der Velden S, Manca M, van der Loos CM, Biessen EAL, et al. Distribution of macrophage polarization markers in human atherosclerosis. *Atherosclerosis*. 2012 Dec;225(2):461–8.
39. Antebi YE, Reich-Zeliger S, Hart Y, Mayo A, Eizenberg I, Rimer J, et al. Mapping differentiation under mixed culture conditions reveals a tunable continuum of T cell fates. *PLoS Biol*. 2013 Jul;11(7):e1001616.
40. Zhou JX, Huang S. Understanding gene circuits at cell-fate branch points for rational cell reprogramming. *Trends Genet*. 2011 Feb;27(2):55–62.
41. Sica A, Mantovani A. Macrophage plasticity and polarization: in vivo veritas. *J Clin Invest*. 2012 Mar;122(3):787–95.
42. Lawrence T, Natoli G. Transcriptional regulation of macrophage polarization: enabling diversity with identity. *Nat Rev Immunol*. 2011 Nov;11(11):750–61.
43. Davis MJ, Tsang TM, Qiu Y, Dayrit JK, Freij JB, Huffnagle GB, et al. Macrophage M1/M2 Polarization Dynamically Adapts to Changes in Cytokine Microenvironments in *Cryptococcus neoformans* Infection. *mBio*. 2013 Jun 18;4(3):e00264-13-e00264-13.
44. Porcheray F, Viaud S, Rimaniol A-C, Leone C, Samah B, Dereuddre-Bosquet N, et al. Macrophage activation switching: an asset for the resolution of inflammation. *Clin Exp Immunol*. 2005 Oct 6;142(12):481–9.
45. Khallou-Laschet J, Varthaman A, Fornasa G, Compain C, Gaston A-T, Clement M, et al. Macrophage Plasticity in Experimental Atherosclerosis. Fritz JH, editor. *PLoS ONE*. 2010 Jan 25;5(1):e8852.
46. Alvarez MM, Liu JC, Trujillo-de Santiago G, Cha B-H, Vishwakarma A, Ghaemmaghami AM, et al. Delivery strategies to control inflammatory response: Modulating M1–M2 polarization in tissue engineering applications. *Journal of Controlled Release* [Internet]. 2016 Jan [cited 2016 Feb 18]; Available from: <http://linkinghub.elsevier.com/retrieve/pii/S0168365916300232>
47. Moore KJ, Sheedy FJ, Fisher EA. Macrophages in atherosclerosis: a dynamic balance. *Nat Rev Immunol*. 2013 Sep 2;13(10):709–21.
48. Medbury HJ, Williams H, Fletcher JP. Clinical significance of macrophage phenotypes in cardiovascular disease. *Clinical and Translational Medicine* [Internet]. 2014 Dec [cited 2015 Oct 20];3(1). Available from: <http://www.clintransmed.com/content/3/1/63>
49. van der Valk FM, van Wijk DF, Stroes ESG. Novel anti-inflammatory strategies in atherosclerosis. *Curr Opin Lipidol*. 2012 Dec;23(6):532–9.

50. Liu M, Luo F, Ding C, Albeituni S, Hu X, Ma Y, et al. Dectin-1 Activation by a Natural Product Beta-Glucan Converts Immunosuppressive Macrophages into an M₁-like Phenotype. *J Immunol.* 2015 Oct 9;195(10):5055–65.
51. Pelegrin P, Surprenant A. Dynamics of macrophage polarization reveal new mechanism to inhibit IL-1 β release through pyrophosphates. *The EMBO Journal.* 2009 Jul 22;28(14):2114–27.
52. Mariani L, Löhning M, Radbruch A, Höfer T. Transcriptional control networks of cell differentiation: insights from helper T lymphocytes. *Prog Biophys Mol Biol.* 2004 Sep;86(1):45–76.
53. Hong T, Xing J, Li L, Tyson JJ. A simple theoretical framework for understanding heterogeneous differentiation of CD4⁺ T cells. *BMC Syst Biol.* 2012;6:66.
54. Carballo E. Feedback Inhibition of Macrophage Tumor Necrosis Factor- Production by Tristetraprolin. *Science.* 1998 Aug 14;281(5379):1001–5.
55. Liu H, Sidiropoulos P, Song G, Pagliari LJ, Birrer MJ, Stein B, et al. TNF-alpha Gene Expression in Macrophages: Regulation by NF kappa B Is Independent of c-Jun or C/EBP. *The Journal of Immunology.* 2000 Apr 15;164(8):4277–85.
56. Sadtler K, Allen BW, Estrellas K, Housseau F, Pardoll DM, Elisseff JH. The Scaffold Immune Microenvironment: Biomaterial-Mediated Immune Polarization in Traumatic and Nontraumatic Applications. *Tissue Engineering Part A [Internet].* 2016 Nov 9 [cited 2016 Dec 19]; Available from: <http://online.liebertpub.com/doi/10.1089/ten.tea.2016.0304>
57. Fuchs A-K, Syrovets T, Haas KA, Loos C, Musyanovych A, Mailänder V, et al. Carboxyl- and amino-functionalized polystyrene nanoparticles differentially affect the polarization profile of M₁ and M₂ macrophage subsets. *Biomaterials.* 2016 Apr;85:78–87.
58. Dong P, Ma L, Liu L, Zhao G, Zhang S, Dong L, et al. CD86⁺/CD206⁺, Diametrically Polarized Tumor-Associated Macrophages, Predict Hepatocellular Carcinoma Patient Prognosis. *Int J Mol Sci.* 2016;17(3).
59. Kadl A, Meher AK, Sharma PR, Lee MY, Doran AC, Johnstone SR, et al. Identification of a novel macrophage phenotype that develops in response to atherogenic phospholipids via Nrf2. *Circ Res.* 2010 Sep 17;107(6):737–46.
60. Ohmori Y, Hamilton TA. Interleukin-4/STAT6 represses STAT1 and NF-kappa B-dependent transcription through distinct mechanisms. *J Biol Chem.* 2000 Dec 1;275(48):38095–103.

61. Kristof AS, Marks-Konczalik J, Billings E, Moss J. Stimulation of signal transducer and activator of transcription-1 (STAT1)-dependent gene transcription by lipopolysaccharide and interferon-gamma is regulated by mammalian target of rapamycin. *J Biol Chem.* 2003 Sep 5;278(36):33637-44.
62. Szanto A, Balint BL, Nagy ZS, Barta E, Dezso B, Pap A, et al. STAT6 transcription factor is a facilitator of the nuclear receptor PPAR γ -regulated gene expression in macrophages and dendritic cells. *Immunity.* 2010 Nov 24;33(5):699-712.
63. Hu X, Chakravarty SD, Ivashkiv LB. Regulation of interferon and Toll-like receptor signaling during macrophage activation by opposing feedforward and feedback inhibition mechanisms. *Immunol Rev.* 2008 Dec;226:41-56.
64. Lowenstein CJ, Padalko E. iNOS (NOS2) at a glance. *J Cell Sci.* 2004 Jun 15;117(Pt 14):2865-7.
65. Messner B, Stütz AM, Albrecht B, Peiritsch S, Woisetschläger M. Cooperation of binding sites for STAT6 and NF kappa B/rel in the IL-4-induced up-regulation of the human IgE germline promoter. *J Immunol.* 1997 Oct 1;159(7):3330-7.
66. Abu-Amer Y. IL-4 abrogates osteoclastogenesis through STAT6-dependent inhibition of NF-kappaB. *J Clin Invest.* 2001 Jun;107(11):1375-85.
67. Shen CH, Stavnezer J. Interaction of stat6 and NF-kappaB: direct association and synergistic activation of interleukin-4-induced transcription. *Mol Cell Biol.* 1998 Jun;18(6):3395-404.
68. Goenka S, Kaplan MH. Transcriptional regulation by STAT6. *Immunol Res.* 2011 May;50(1):87-96.
69. Malyshev I, Malyshev Y. Current Concept and Update of the Macrophage Plasticity Concept: Intracellular Mechanisms of Reprogramming and M3 Macrophage "Switch" Phenotype. *BioMed Research International.* 2015;2015:1-22.
70. Mokarram N, Merchant A, Mukhatyar V, Patel G, Bellamkonda RV. Effect of modulating macrophage phenotype on peripheral nerve repair. *Biomaterials.* 2012 Dec;33(34):8793-801.
71. Spiller KL, Nassiri S, Witherel CE, Anfang RR, Ng J, Nakazawa KR, et al. Sequential delivery of immunomodulatory cytokines to facilitate the M1-to-M2 transition of macrophages and enhance vascularization of bone scaffolds. *Biomaterials.* 2015 Jan;37:194-207.
72. Warnes GR, Bolker B, Bonebakker L, Gentleman R, Huber W, Liaw A, et al. gplots: Various R Programming Tools for Plotting Data. [Internet]. 2015. Available from: <https://CRAN.R-project.org/package=gplots>

73. Laurell H, Iacovoni JS, Abot A, Svec D, Maoret J-J, Arnal J-F, et al. Correction of RT-qPCR data for genomic DNA-derived signals with ValidPrime. *Nucleic Acids Res.* 2012 Apr;40(7):e51.
74. Ye J, Coulouris G, Zaretskaya I, Cutcutache I, Rozen S, Madden TL. Primer-BLAST: A tool to design target-specific primers for polymerase chain reaction. *BMC Bioinformatics.* 2012;13(1):134.
75. Vandesompele J, De Preter K, Pattyn F, Poppe B, Van Roy N, De Paepe A, et al. Accurate normalization of real-time quantitative RT-PCR data by geometric averaging of multiple internal control genes. *Genome Biol.* 2002 Jun 18;3(7):research0034.
76. Burnham KP, Anderson DR. Model selection and multimodel inference: a practical information-theoretic approach. 2. ed. New York, NY: Springer; 2010. 488 p.
77. Bellingan GJ, Caldwell H, Howie SE, Dransfield I, Haslett C. In vivo fate of the inflammatory macrophage during the resolution of inflammation: inflammatory macrophages do not die locally, but emigrate to the draining lymph nodes. *J Immunol.* 1996 Sep 15;157(6):2577-85.
78. Libby P. Inflammation in Atherosclerosis. *Arteriosclerosis, Thrombosis, and Vascular Biology.* 2012 Sep 1;32(9):2045-51.
79. Verollet C, Souriant S, Bonnaud E, Jolicoeur P, Raynaud-Messina B, Kinnaer C, et al. HIV-1 reprograms the migration of macrophages. *Blood.* 2015 Mar 5;125(10):1611-22.
80. Prieto J, Eklund A, Patarroyo M. Regulated expression of integrins and other adhesion molecules during differentiation of monocytes into macrophages. *Cell Immunol.* 1994 Jun;156(1):191-211.
81. Harburger DS, Calderwood DA. Integrin signalling at a glance. *Journal of Cell Science.* 2009 Jan 15;122(2):159-63.
82. Brown EJ. Integrins of Macrophages and Macrophage-Like Cells. In: Gordon S, editor. *The Macrophage as Therapeutic Target* [Internet]. Berlin, Heidelberg: Springer Berlin Heidelberg; 2003 [cited 2016 May 4]. p. 111-30. Available from: http://link.springer.com/10.1007/978-3-642-55742-2_7
83. Bellingan GJ, Xu P, Cooksley H, Cauldwell H, Shock A, Bottoms S, et al. Adhesion molecule-dependent mechanisms regulate the rate of macrophage clearance during the resolution of peritoneal inflammation. *J Exp Med.* 2002 Dec 2;196(11):1515-21.
84. Cao C, Lawrence DA, Strickland DK, Zhang L. A specific role of integrin Mac-1 in accelerated macrophage efflux to the lymphatics. *Blood.* 2005 Nov 1;106(9):3234-41.

85. Monick MM, Powers L, Butler N, Yarovinsky T, Hunninghake GW. Interaction of matrix with integrin receptors is required for optimal LPS-induced MAP kinase activation. *American Journal of Physiology - Lung Cellular and Molecular Physiology*. 2002 Aug 1;283(2):L390-402.
86. Berton G, Lowell CA. Integrin Signalling in Neutrophils and Macrophages. *Cellular Signalling*. 1999 Sep;11(9):621-35.
87. Hind LE, Mackay JL, Cox D, Hammer DA. Two-dimensional motility of a macrophage cell line on microcontact-printed fibronectin. *Cytoskeleton (Hoboken)*. 2014 Sep;71(9):542-54.
88. Hind LE, Lurier EB, Dembo M, Spiller KL, Hammer DA. Effect of M1-M2 Polarization on the Motility and Traction Stresses of Primary Human Macrophages. *Cellular and Molecular Bioengineering*. 2016 Sep;9(3):455-65.
89. DiMilla PA, Barbee K, Lauffenburger DA. Mathematical model for the effects of adhesion and mechanics on cell migration speed. *Biophys J*. 1991 Jul;60(1):15-37.
90. Mas-Moruno C, Rechenmacher F, Kessler H. Cilengitide: the first anti-angiogenic small molecule drug candidate design, synthesis and clinical evaluation. *Anticancer Agents Med Chem*. 2010 Dec;10(10):753-68.
91. Wheeler AP, Wells CM, Smith SD, Vega FM, Henderson RB, Tybulewicz VL, et al. Rac1 and Rac2 regulate macrophage morphology but are not essential for migration. *J Cell Sci*. 2006 Jul 1;119(Pt 13):2749-57.
92. Hayman EG, Pierschbacher MD, Ohgren Y, Ruoslahti E. Serum spreading factor (vitronectin) is present at the cell surface and in tissues. *Proc Natl Acad Sci USA*. 1983 Jul;80(13):4003-7.
93. Pankov R, Endo Y, Even-Ram S, Araki M, Clark K, Cukierman E, et al. A Rac switch regulates random versus directionally persistent cell migration. *The Journal of Cell Biology*. 2005 Aug 29;170(5):793-802.
94. Dütting S, Heidenreich J, Cherpokova D, Amin E, Zhang S-C, Ahmadian MR, et al. Critical off-target effects of the widely used Rac1 inhibitors NSC23766 and EHT1864 in mouse platelets. *J Thromb Haemost*. 2015 May;13(5):827-38.
95. Levay M, Krobert KA, Wittig K, Voigt N, Bermudez M, Wolber G, et al. NSC23766, a widely used inhibitor of Rac1 activation, additionally acts as a competitive antagonist at muscarinic acetylcholine receptors. *J Pharmacol Exp Ther*. 2013 Oct;347(1):69-79.
96. Sturge J, Todd SK, Kogianni G, McCarthy A, Isacke CM. Mannose receptor regulation of macrophage cell migration. *Journal of Leukocyte Biology*. 2007 Jun 26;82(3):585-93.

97. Wheeler AP, Ridley AJ. RhoB affects macrophage adhesion, integrin expression and migration. *Experimental Cell Research*. 2007 Oct;313(16):3505–16.
98. Codling EA, Plank MJ, Benhamou S. Random walk models in biology. *Journal of The Royal Society Interface*. 2008 Aug 6;5(25):813–34.
99. Wu P-H, Giri A, Sun SX, Wirtz D. Three-dimensional cell migration does not follow a random walk. *Proc Natl Acad Sci USA*. 2014 Mar 18;111(11):3949–54.
100. Wu P-H, Giri A, Wirtz D. Statistical analysis of cell migration in 3D using the anisotropic persistent random walk model. *Nature Protocols*. 2015 Feb 26;10(3):517–27.
101. Fuhrmann A, Engler AJ. Acute shear stress direction dictates adherent cell remodeling and verifies shear profile of spinning disk assays. *Physical Biology*. 2015 Jan 26;12(1):16011.
102. Maridonneau-Parini I. Control of macrophage 3D migration: a therapeutic challenge to limit tissue infiltration. *Immunological Reviews*. 2014 Nov;262(1):216–31.
103. Du J, Paz K, Flynn R, Vulic A, Robinson TM, Lineburg KE, et al. Pirfenidone ameliorates murine chronic GVHD through inhibition of macrophage infiltration and TGF- β production. *Blood*. 2017 Mar 2;blood-2017-01-758854.
104. Zaveri TD, Lewis JS, Dolgova NV, Clare-Salzler MJ, Keselowsky BG. Integrin-directed modulation of macrophage responses to biomaterials. *Biomaterials*. 2014 Apr;35(11):3504–15.
105. Efimenko K, Wallace WE, Genzer J. Surface Modification of Sylgard-184 Poly(dimethyl siloxane) Networks by Ultraviolet and Ultraviolet/Ozone Treatment. *Journal of Colloid and Interface Science*. 2002 Oct;254(2):306–15.
106. Meijering E, Dzyubachyk O, Smal I. Methods for Cell and Particle Tracking. In: *Methods in Enzymology* [Internet]. Elsevier; 2012 [cited 2017 Mar 8]. p. 183–200. Available from: <http://linkinghub.elsevier.com/retrieve/pii/B9780123918574000094>
107. Van Goethem E, Poincloux R, Gauffre F, Maridonneau-Parini I, Le Cabec V. Matrix architecture dictates three-dimensional migration modes of human macrophages: differential involvement of proteases and podosome-like structures. *Journal of immunology (Baltimore, Md : 1950)*. 2010 Jan;184(2):1049–61.
108. Cougoule C, Van Goethem E, Le Cabec V, Lafouresse F, Dupré L, Mehraj V, et al. Blood leukocytes and macrophages of various phenotypes have distinct abilities to form podosomes and to migrate in 3D environments. *European journal of cell biology*. 2012;91(11–12):938–49.

109. Wiesner C, Le-Cabec V, El Azzouzi K, Maridonneau-Parini I, Linder S. Podosomes in space: macrophage migration and matrix degradation in 2D and 3D settings. *Cell Adh Migr*. 2014;8(3):179–91.
110. Campos D, Méndez V, Llopis I. Persistent random motion: Uncovering cell migration dynamics. *Journal of Theoretical Biology*. 2010 Dec;267(4):526–34.
111. El Kasmi KC, Qualls JE, Pesce JT, Smith AM, Thompson RW, Henao-Tamayo M, et al. Toll-like receptor–induced arginase 1 in macrophages thwarts effective immunity against intracellular pathogens. *Nature Immunology*. 2008 Dec;9(12):1399–406.
112. Wynn TA, Barron L. Macrophages: master regulators of inflammation and fibrosis. *Semin Liver Dis*. 2010 Aug;30(3):245–57.
113. Lameijer MA, Tang J, Nahrendorf M, Beelen RHJ, Mulder WJM. Monocytes and macrophages as nanomedicinal targets for improved diagnosis and treatment of disease. *Expert Review of Molecular Diagnostics*. 2013 Jul;13(6):567–80.
114. Linde N, Gutschalk CM, Hoffmann C, Yilmaz D, Mueller MM. Integrating Macrophages into Organotypic Co-Cultures: A 3D In Vitro Model to Study Tumor-Associated Macrophages. Lisanti M, editor. *PLoS ONE*. 2012 Jul 6;7(7):e40058.
115. Müller-Quernheim UC, Potthast L, Müller-Quernheim J, Zissel G. Tumor-cell co-culture induced alternative activation of macrophages is modulated by interferons in vitro. *J Interferon Cytokine Res*. 2012 Apr;32(4):169–77.
116. Roudnicky F, Hollmén M. Transcriptional profiling of macrophage and tumor cell interactions in vitro. *Genomics Data*. 2016 Jun;8:1–3.
117. Hollmén M, Roudnicky F, Karaman S, Detmar M. Characterization of macrophage - cancer cell crosstalk in estrogen receptor positive and triple-negative breast cancer. *Scientific Reports*. 2015 Mar 17;5:9188.
118. Dwyer AR, Ellies LG, Holme AL, Pixley FJ. A three-dimensional co-culture system to investigate macrophage-dependent tumor cell invasion. *Journal of Biological Methods*. 2016 Jul 24;3(3):49.
119. Beachley VZ, Wolf MT, Sadtler K, Manda SS, Jacobs H, Blatchley MR, et al. Tissue matrix arrays for high-throughput screening and systems analysis of cell function. *Nature Methods*. 2015 Oct 19;12(12):1197–204.
120. Cassetta L, Noy R, Swierczak A, Sugano G, Smith H, Wiechmann L, et al. Isolation of Mouse and Human Tumor-Associated Macrophages. *Adv Exp Med Biol*. 2016;899:211–29.

121. Laoui D, Overmeire E, Keirse J, Movahedi K, Ginderachter J. Purification of Tumor-Associated Macrophages (TAM) and Tumor-Associated Dendritic Cells (TADC). BIO-PROTOCOL [Internet]. 2014 [cited 2017 Mar 13];4(22). Available from: <http://www.bio-protocol.org/e1294>
122. Zaveri TD, Dolgova NV, Lewis JS, Hamaker K, Clare-Salzler MJ, Keselowsky BG. Macrophage integrins modulate response to ultra-high molecular weight polyethylene particles and direct particle-induced osteolysis. *Biomaterials*. 2017 Jan;115:128–40.

Appendix A. Supplement to Chapter 2

We constructed mathematical models comprising minimal nonlinear Ordinary Differential Equation (ODE) networks. Our models were developed from previously described models of T cell subset specialization,¹⁻³ adding additional connectivities and species to account for the complex kinetics of CD86 and CD206 after stimulation. We constructed 70 models with different topologies. A representative set of the studied topologies, models 1-6, are illustrated in Figure 2 and Supplementary Figure A4. A model described by the mutual-inhibition self-activation (MISA) motif (Model 2) fits the data better than one in which the M₁- and M₂-associated pathways are activated independently (Model 1). However, the MISA is nevertheless insufficient to capture the complex kinetics of CD86 and CD206 expression after co-stimulation.

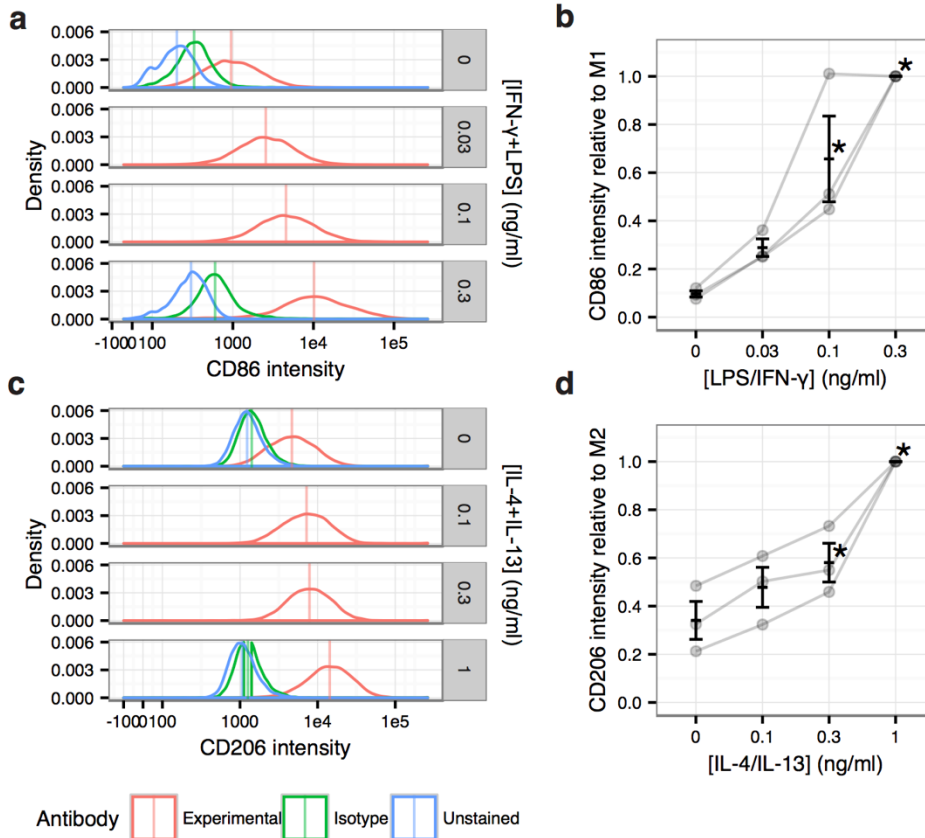
Models that extend the MISA topology by introducing a new species Y that interacts with the M₁- and M₂-associated pathways, and representing unknown processes downstream of LPS+IFN- γ and/or IL-4+IL-13 signalling events improve the model score (see AICc below) (Models 3, 5, 6). Specifically, we found that an incoherent feed-forward loop on M₁, mediated by an additional species Y, was necessary to capture the decay of CD86 expression in costimulated cells at 96 hours.⁴ An activating link between Y and M₂ was also consistent with the increased expression of CD206 of costimulated cells at later times. In particular, cooperative activation of M₂ from Y and M₂ improved the overall fit. To discover extended topologies, we were guided by the features of the temporal data and the literature on macrophage activation, as discussed in the main text.

Model quality was assessed based on optimization of parameters by fitting to the 96-hour time course data (Fig. 2) of four timepoints (24, 48, 72, 96 h) for four different stimulation conditions ($\{0.3,0\}$, $\{0.3,1\}$, $\{0,0\}$, $\{0,1\}$ ng/ml {LPS/IFN- γ , IL-4/IL-13}). The number of replicates was between three and five for each timepoint, giving 72 experimental data points. The error metric used was the sum of squared residuals (RSS) with normalized mean weighting. Parameter estimation was performed by minimizing the RSS of the model predicted CD86 and CD206 values to the normalized mean-weighted experimental values. The Matlab Optimization Toolbox and the trust-region-reflective algorithm were used to perform 1,000 individual fits. Parameters were initialized from a lognormal distribution with a mean and variance of 2, and were constrained to be positive. Parameters were optimized to the normalized timecourse data, and thus are expressed in arbitrary concentration and time units. Initial fits were performed using 400 trust-region-reflective iterations, or until convergence, using normalized unweighted experimental values. A second fit was then performed to the normalized mean-weighted experimental values. All models were assessed using the AICc criterion, a scoring metric for model selection that includes penalties for increasing the number of fitted parameters.⁵

To replicate the cell-to-cell variability in the flow cytometry data, individual cells were given static parameters drawn from a distribution. Cell populations with between 3000 and 10000 cells were simulated, and model parameters for each cell were drawn from a lognormal distribution centered on the optimized parameters and with a variance of one percent of the mean. The resulting CD86 and CD206 expression levels for all models in Figure 2 and fitted parameters (Supplementary Figure A4) showed single-peaked

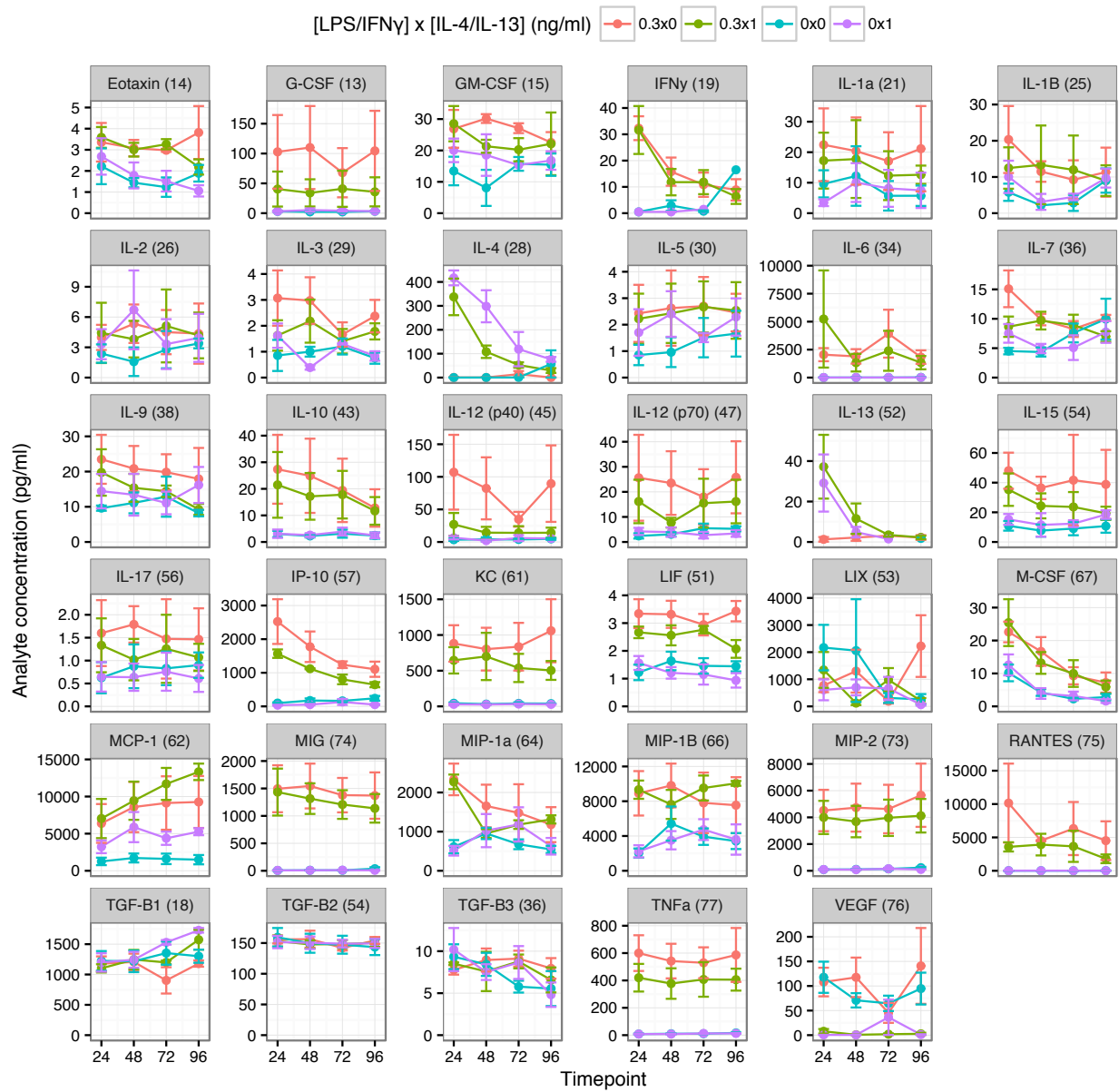
distributions shifting with dosage, in qualitative agreement with the experimental density plots.

A.1. Supplementary Figures

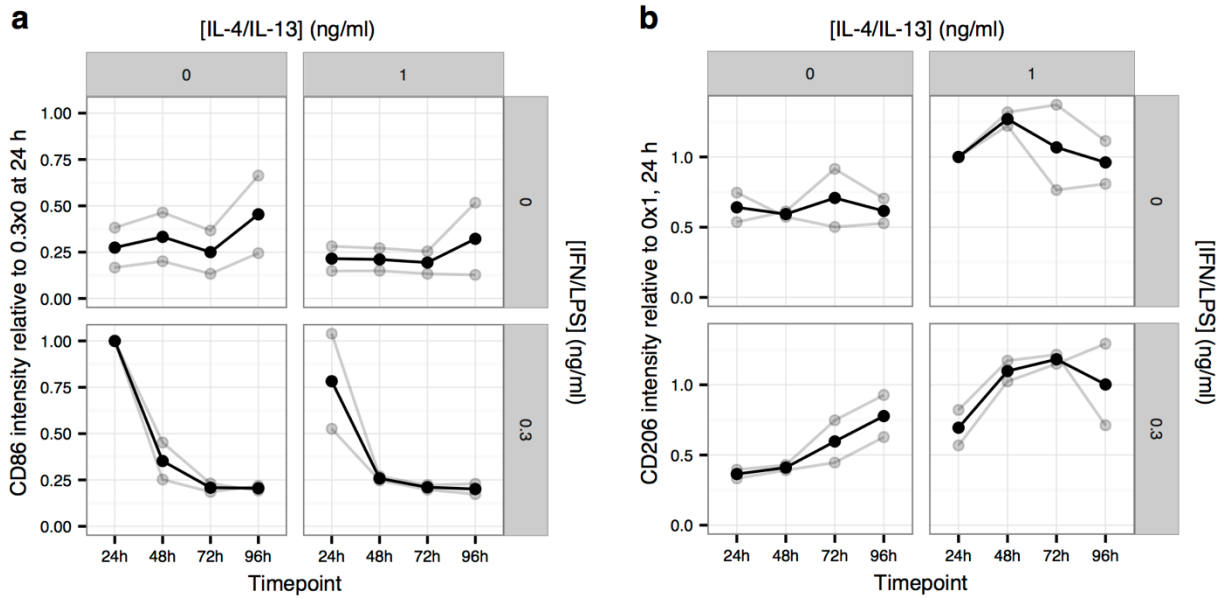


Supplementary Figure A1. Expression of phenotypic markers CD86 and CD206 in response to LPS+IFN- γ and IL-4+IL-13 stimuli is dose-dependent.

(A) Representative flow cytometry histograms of CD86 intensity after 48 hours of treatment with indicated dose of LPS+IFN- γ . (B) Average median normalized CD86 expression \pm SEM as a function of increasing LPS+IFN- γ dose. Data are normalized to 0.3 ng/ml treatment condition. Asterisk indicates difference vs. untreated, $p < 0.05$; $n = 3$. (C) Representative flow cytometry histograms of CD206 intensity after 48 hours of treatment with indicated dose of IL-4+IL-13. (D) Average median normalized CD206 intensity \pm SEM as a function of increasing IL-4+IL-13 dose. Data are normalized to 1 ng/ml treatment condition. Asterisk indicates difference vs. untreated by two-sided t test, $p < 0.05$; $n = 3$.

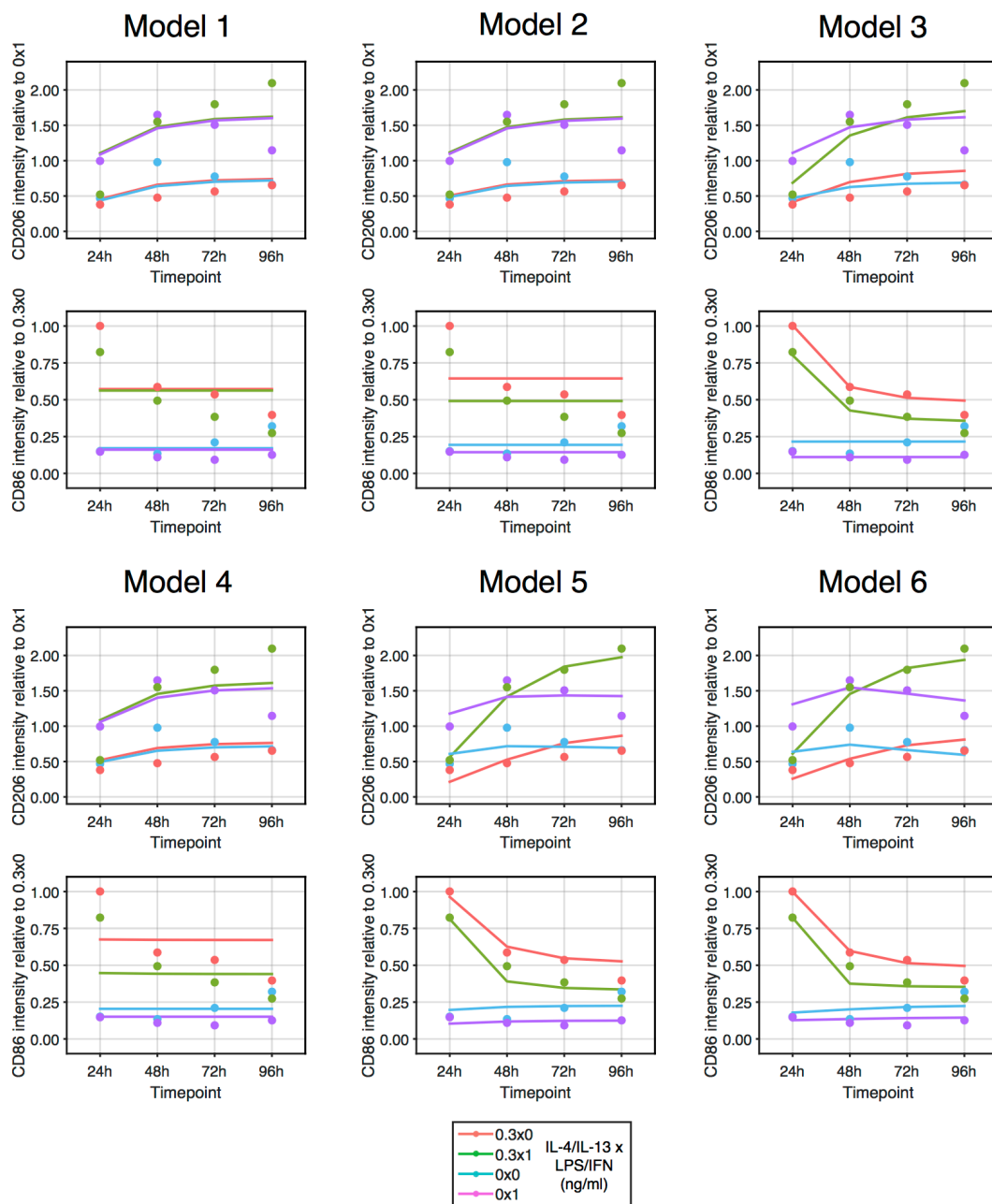


Supplementary Figure A2. Cytokines present in culture media of macrophages exposed to LPS+IFN- γ \pm IL-4+IL-13 for the indicated time in hours, assessed by multiplex ELISA. Data presented as mean \pm SEM, $n=3$.

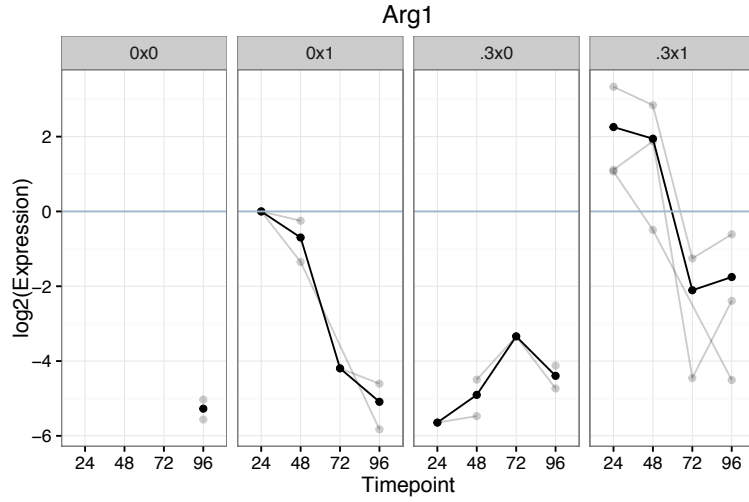


Supplementary Figure A3. Pulse-chase experiment.

Cells were treated with LPS+IFN- γ or IL-4+IL-13 at t=0. Media was replaced with untreated media at t=24 hours. Cells were collected at t=24, 48, 72, and 96 hours for analysis of CD86 and CD206 expression by flow cytometry to observe how marker expression evolved over time in the absence of continued stimulus. Median normalized fluorescence intensity from each experiment (n=2) is plotted in gray and the mean is plotted in black.



Supplementary Figure A4. Simulated timecourse experiment from each model shown in Figure 2.3. Points mark experimental data, as shown in Figure 2.3b.



Supplementary Figure A5. qRT-PCR timecourse data for Arg1 expression, relative to the IL-4+IL-13-only condition at 24 hours.

Gray points are individual observations and gray lines connect points from the same experiment; the black points and line represent the average. Missing points indicate missing data due to signals below limit of quantitation. Headings describe stimulation condition as ng/ml concentration of LPS/IFN- γ x IL-4/IL-13. Timepoint is in hours.

A.2. Supplementary Equations

The parameters of these equations are described in Supplementary Table A2 and fitted numeric values are given in Supplementary Table A3.

Equation A1. Model 1: Self-activation

$$\frac{d[M1]}{dt} = k_1 \frac{S1}{S1 + K_{ind1}} + k_3 \frac{[M1]}{[M1] + K_{act}} + k_5 - d_1[M1]$$

$$\frac{d[M2]}{dt} = k_2 \frac{S2}{S2 + K_{ind2}} + k_4 \frac{[M2]}{[M2] + K_{act}} + k_6 - d_2[M2]$$

$$\frac{d[CD86]}{dt} = g_1[M1] - d_4[CD86]$$

$$\frac{d[CD206]}{dt} = g_2[M2] - d_5[CD206]$$

Equation A2. Model 2: MISA

$$\frac{d[M1]}{dt} = \frac{k_1 \frac{S1}{S1 + K_{ind1}} + k_3 \frac{[M1]}{[M1] + K_{act}}}{1 + ([M2] / K_{rep2})^n} + k_5 - d_1[M1]$$

$$\frac{d[M2]}{dt} = \frac{k_2 \frac{S2}{S2 + K_{ind2}} + k_4 \frac{[M2]}{[M2] + K_{act}}}{1 + ([M1] / K_{rep1})^n} + k_6 - d_2[M2]$$

$$\frac{d[CD86]}{dt} = g_1[M1] - d_4[CD86]$$

$$\frac{d[CD206]}{dt} = g_2[M2] - d_5[CD206]$$

Equation A3. Model 3: MISA with IFFL and inhibition between Y and M1

$$\frac{d[M1]}{dt} = \frac{k_1 \frac{S1}{S1+K_{ind1}} + k_3 \frac{[M1]}{[M1]+K_{act}}}{(1 + ([M2]/K_{rep2})^n) (1 + ([Y]/K_Y)^n)} + k_5 - d_1[M1]$$

$$\frac{d[M2]}{dt} = \frac{k_2 \frac{S2}{S2+K_{ind2}} + k_4 \frac{[M2]}{[M2]+K_{act}}}{(1 + ([M1]/K_{rep1})^n)} + k_6 + k_7 \frac{[Y]}{[Y] + K_{CY}} - d_2[M2]$$

$$\frac{d[Y]}{dt} = k_8 \frac{S1}{S1 + K_{ind1}} - d_3[Y]$$

$$\frac{d[CD86]}{dt} = g_1[M1] - d_4[CD86]$$

$$\frac{d[CD206]}{dt} = g_2[M2] - d_5[CD206]$$

Equation A4. Model 4: MISA with cooperative IFFL

$$\frac{d[M1]}{dt} = \frac{k_1 \frac{S1}{S1+K_{ind1}} + k_3 \frac{[M1]}{[M1]+K_{act}}}{(1 + ([M2]/K_{rep2})^n)} + k_5 - d_1[M1]$$

$$\frac{d[M2]}{dt} = \frac{k_2 \frac{S2}{S2+K_{ind2}} + k_4 \frac{[M2]}{[M2]+K_{act}} + k_7 \frac{[M2][Y]}{(K_{CM2}+[M2])(K_{CY}+[Y])}}{(1 + ([M1]/K_{rep1})^n)} + k_6 - d_2[M2]$$

$$\frac{d[Y]}{dt} = k_8 \frac{S1}{S1 + K_{ind1}} - d_3[Y]$$

$$\frac{d[CD86]}{dt} = g_1[M1] - d_4[CD86]$$

$$\frac{d[CD206]}{dt} = g_2[M2] - d_5[CD206]$$

Equation A5. Model 5: MISA with cooperative IFFL and inhibition between Y and M₁

$$\frac{d[M1]}{dt} = \frac{k_1 \frac{S1}{S1+K_{ind1}} + k_3 \frac{[M1]}{[M1]+K_{act}}}{\left(1 + ([M2]/K_{rep2})^n\right) \left(1 + ([Y]/K_Y)^n\right)} + k_5 - d_1[M1]$$

$$\frac{d[M2]}{dt} = \frac{k_2 \frac{S2}{S2+K_{ind2}} + k_4 \frac{[M2]}{[M2]+K_{act}} + k_7 \frac{[M2][Y]}{(K_{CM2}+[M2])(K_{CY}+[Y])}}{\left(1 + ([M1]/K_{rep1})^n\right)} + k_6 - d_2[M2]$$

$$\frac{d[Y]}{dt} = k_8 \frac{S1}{S1 + K_{ind1}} - d_3[Y]$$

$$\frac{d[CD86]}{dt} = g_1[M1] - d_4[CD86]$$

$$\frac{d[CD206]}{dt} = g_2[M2] - d_5[CD206]$$

Equation A6. Model 6: MISA with cooperative IFFL, inhibition between Y and M₁, and inhibition on Y

$$\frac{d[M1]}{dt} = \frac{k_1 \frac{S1}{S1+K_{ind1}} + k_3 \frac{[M1]}{[M1]+K_{act}}}{\left(1 + ([M2]/K_{rep2})^n\right) \left(1 + ([Y]/K_Y)^n\right)} + k_5 - d_1[M1]$$

$$\frac{d[M2]}{dt} = \frac{k_2 \frac{S2}{S2+K_{ind2}} + k_4 \frac{[M2]}{[M2]+K_{act}} + k_7 \frac{[M2][Y]}{(K_{CM2}+[M2])(K_{CY}+[Y])}}{\left(1 + ([M1]/K_{rep1})^n\right)} + k_6 - d_2[M2]$$

$$\frac{d[Y]}{dt} = \frac{k_8 \frac{S1}{S1+K_{ind1}}}{1 + (S2/K_{ind2})^n} - d_3[Y]$$

$$\frac{d[CD86]}{dt} = g_1[M1] - d_4[CD86]$$

$$\frac{d[CD206]}{dt} = g_2[M2] - d_5[CD206]$$

A.3. Supplementary Tables

Supplementary Table A1. qPCR primers

Gene	Direction	Sequence	Amplicon length (bp)
Arg1	F	CTCTGTCTTTTAGGGTTACGG	152
	R	CTCGAGGCTGTCCTTTTGAG	
Chi3l3	F	AGTGCTGATCTCAATGTGGATTC	142
	R	TAGGGGCACCAATTCCAGTC	
Gapdh	F	GTCAAGCTCATTTCCTGGTATGAC	131
	R	TCTCTTGCTCAGTGTCTTGC	
Hprt	F	TGGACAGGACTGAAAGACTTGCTCG	81
	R	CCTTGAGCACACAGAGGGCCAC	
Ilio	F	CCCACTTCCCAGTCGGCCAG	300
	R	GGAGAAATCGATGACAGCGCCTC	
Kdm6b	F	GGTTCAC TTCGGCTCAACTTAG	75
	R	CTCCACCGTATGTTACCGC	
Ldha ^A	F	TGTCTCCAGCAAAGACTACTGT	155
	R	GACTGTACTTGACAATGTTGGGA	
Mrc1	F	TGTTTTGGTTGGGACTGACC	269
	R	TGCAGTAACTGGTGGATTGTC	
mVPA1 ⁶	F	GGAGCCCAGTGTAGAAGAGCA	87
	R	AGCCAGCGAACCATATCCTGA	
Nos2	F	TTGGGTCTTGTTCACTCCAC	211
	R	TGTATTGTTGGGCTGAGAACAG	
Retnla	F	GCCAATCCAGCTAACTATCCC	187
	R	AGTCAACGAGTAAGCACAGG	
Sdha ^B	F	CTTGAATGAGGCTGACTGTG	87
	R	ATCACATAAGCTGGTCCTGT	
Tnfa	F	CCCACGTCGTAGCAAACCACCA	172
	R	TCGGGGCAGCCTTGTCCCTT	

^A RTPrimerDB⁷ 3720; ^B RTPrimerDB 3875

Supplementary Table A2. Description of model parameters

Parameter	Meaning
k_1	Maximum stimulation rate of M1 cascade under induction with S1
k_2	Maximum stimulation rate of M2 cascade under induction with S2
k_3	Maximum stimulation rate of M1 cascade under self-activation
k_4	Maximum stimulation rate of M2 cascade under self-activation
k_5	Basal rate of M1 activation
k_6	Basal rate of M2 activation
k_7	Maximum rate of M2 stimulation from Y and M2 cooperative stimulation
k_8	Maximum rate of Y production under S1 induction
K_Y	Level of Y to reach half-maximum inhibition of M1
K_{CY}	Level of Y to reach half-maximum cooperative activation of M2
K_{CM2}	Level of M2 to reach half-maximum cooperative activation of M2
K_{rep1}	Level of M1 to reach half-maximum inhibition of M2
K_{rep2}	Level of M2 to reach half-maximum inhibition of M1
K_{ind1}	Level of S1 to reach half-maximum induction of M1
K_{ind2}	Level of S2 to reach half-maximum induction of M2
K_{act}	Level of M1 or M2 to reach half-maximum self-activation
d_1	M1 decay rate
d_2	M2 decay rate
d_3	Y decay rate
d_4	CD86 decay rate
d_5	CD206 decay rate
g_1	CD86 production rate
g_2	CD206 production rate
n	Hill coefficient

Supplementary Table A3. Model parameter values

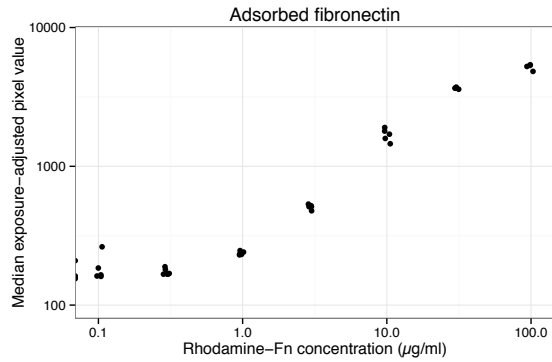
Representative best fit parameter values for each model from optimization. Parameters are in arbitrary units of concentration and time, relative to the rate of degradation of the M1 species (d_1), which is approximated to be 1 [1/hr] according to the half-life of STAT1.⁸ The parameters were optimized to normalized CD86 and CD206 expression levels. Parameters with an asterisk were fixed to constrain parameter space during optimization. Fixed values were chosen based on initial parameter searches. Alternative constraints yielded different quantitative values, but the same ordering of model scores according to the AICc. The threshold parameters for induction, K_{ind1} and K_{ind2} are based on the dose-response of CD86 and CD206 under the single-stimulus conditions. K_{act} is approximated from the experimental data condition with no induction stimulus at 24 hours. A Hill coefficient of 2 was used for all parameter sets. Parameter sets estimated using a Hill coefficient of 1 produced AICc scores equivalent or worse than the AICc scores using a Hill coefficient of 2.

Model	1	2	3	4	5	6
k_1	0.4341	0.5871	10.421	0.7595	2.2698	2.8511
k_2	1.1124	1.6691	1.4815	1.4998	0.8939	1.0146
k_3	0.8322	0.791	1.0512	0.6856	1.1102	0.7833
k_4	1.6865	0.311	0.9216	0.4332	1.5412	1.1121
k_5	0.0456	0.0679	0.0421	0.0968	0.0332	0.1067
k_6	0.0172	0.5813	0.3239	0.541	0.0831	0.1589
k_7	N/A	N/A	0.1977	4.3814	2.8281	2.2411
k_8	N/A	N/A	0.1096	0.1594	0.7288	0.1206
K_{M2}	N/A	N/A	N/A	9.9178	1.3292	0.0012
K_{CY}	N/A	N/A	0.3438	8.4118	5.4604	5.4965
K_Y	N/A	N/A	N/A	N/A	0.0209	0.9182
K_{rep1}	N/A	2.8882	2.2441	1.9004	2.4051	1.0306
K_{rep2}	N/A	14.228	1.4216	2.0858	1.0162	1.195
K_{ind1}^*	1	1	1	1	1	1
K_{ind2}^*	0.3	0.3	0.3	0.3	0.3	0.3
K_{act}^*	1	1	1	1	1	1
d_1^*	1	1	1	1	1	1
d_2^*	1	1	1	1	1	1
d_3^*	N/A	N/A	0.05	0.05	0.05	0.05
d_4^*	0.05	0.05	0.05	0.05	0.05	0.05
d_5^*	0.05	0.05	0.05	0.05	0.05	0.05
g_1^*	1	1	1	1	1	1
g_2^*	1	1	1	1	1	1
n	N/A	2	N/A	2	2	2
Free parameters	6	8	11	12	13	13

A.4. References

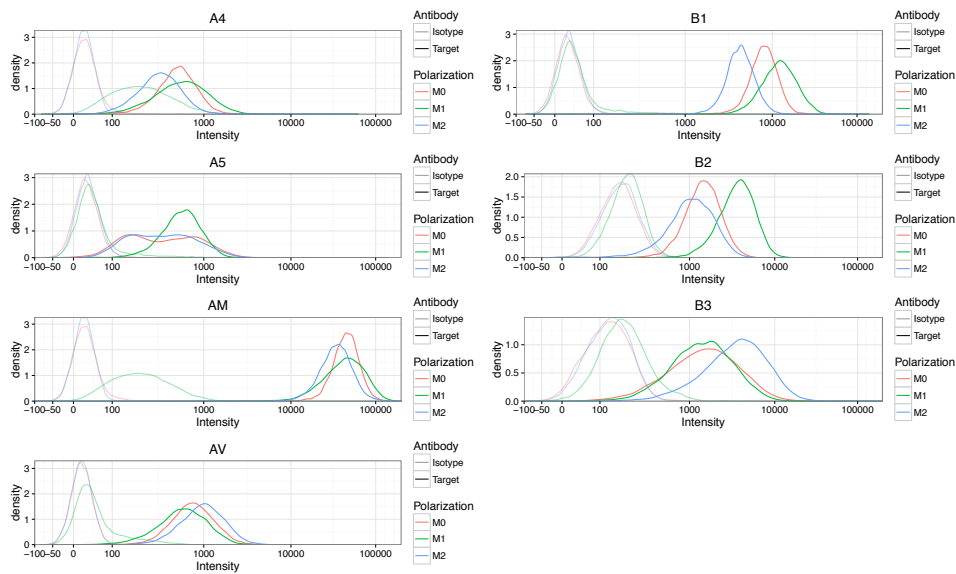
1. Mariani, L., Löhning, M., Radbruch, A. & Höfer, T. Transcriptional control networks of cell differentiation: insights from helper T lymphocytes. *Prog. Biophys. Mol. Biol.* **86**, 45–76 (2004).
2. Hong, T., Xing, J., Li, L. & Tyson, J. J. A simple theoretical framework for understanding heterogeneous differentiation of CD4+ T cells. *BMC Syst Biol* **6**, 66 (2012).
3. Antebi, Y. E. *et al.* Mapping differentiation under mixed culture conditions reveals a tunable continuum of T cell fates. *PLoS Biol.* **11**, e1001616 (2013).
4. Alon, U. *An introduction to systems biology: design principles of biological circuits.* (Chapman & Hall/CRC, 2007).
5. Nelder, J. A. & Mead, R. A Simplex Method for Function Minimization. *The Computer Journal* **7**, 308–313 (1965).
6. Laurell, H. *et al.* Correction of RT-qPCR data for genomic DNA-derived signals with ValidPrime. *Nucleic acids research* **40**, e51–e51 (2012).
7. Lefever, S., Vandesompele, J., Speleman, F. & Pattyn, F. RTPPrimerDB: the portal for real-time PCR primers and probes. *Nucleic Acids Res.* **37**, D942–945 (2009).
8. Legewie, S., Herzel, H., Westerhoff, H. V. & Blüthgen, N. Recurrent design patterns in the feedback regulation of the mammalian signalling network. *Mol. Syst. Biol.* **4**, 190 (2008).

Appendix B. Supplement to Chapter 3

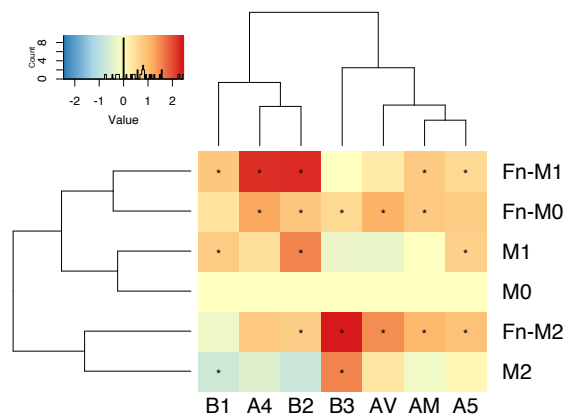


Supplementary Figure B1. Fibronectin adsorption curve.

Fluorescence from surface-bound rhodamine-fibronectin increases with the concentration of the coating solution and begins to saturate between 30 and 100 µg/ml.



Supplementary Figure B2. Representative flow cytometry plots of BMDM integrin expression as a function of macrophage polarization.



Supplementary Figure B3. Integrin expression changes 24 h after macrophage polarization on different ECMs.

Median fluorescence intensity of flow cytometry data, expressed as \log_2 fold expression vs Mo on TCPS.